Preface

"Learn from yesterday, live for today, hope for tomorrow. The important thing is not to stop questioning." (Albert Einstein)

The combination of biology and physics is what makes medical imaging so interesting, especially when it investigates an important disorder like dementia. Performing research in the field of positron emission tomography along with kinetic modeling was a true expedition for me, interesting, fun and challenging. My dissertation is the product of this pleasant but sometimes difficult venture. Without the support and guidance of a number of people, this dissertation would not have been possible. Therefore I would like to thank them.

First of all I want to express my sincere thanks to my promoter Prof. Dr. Patrick Dupont for his very valuable guidance, the productive discussions, his encouragement and believe in me during the whole phase of the thesis project. In addition I wish to thank him for giving me the opportunity to go on a research exchange at the Department of Radiology & Nuclear Medicine of the VU University Medical Centre (VUmc) Amsterdam and having an educational experience.

I take this opening to gratefully thank Prof. Dr. Ronald Boellaard, Dr. Sandeep Golla and the other members of the Department of Radiology & Nuclear Medicine of the VUmc Amsterdam for their valuable time, their expertise, the extremely pleasant cooperation and warm welcome.

I am also grateful to Prof. Dr. Rik Vandenberghe, Prof. Dr. Koen Van Laere, Prof. Dr. Guy Bormans and Dr. Natalie Nelissen to provide me with the retrospective dataset. Likewise I wish to thank Prof. Dr. Mathieu Vandenbulcke and Dr. Jolien Schaeverbeke for their help in gathering the right information about the study data.

Furthermore I would like to express my gratitude towards Prof. Dr. Paul Suetens for my working space in the Medical Imaging Research Center (MIRC). I also want to thank my colleagues at the MIRC of UZ Leuven for the nice atmosphere accompanied with a four o'clock coffee- and fruit break.

To all my friends, for helping me through the thesis-stress but also for the wonderful moments together, thank you.

Most importantly, I want to express my deepest thanks to my mother, father and sister for their endless support, love and patience at any time.

Summary

In vivo quantification of acetylcholinesterase (AchE) in the human brain using PET, a proper tracer and kinetic modeling provides assessment of the cholinergic system. Evaluation of the cholinergic function is important since dysfunction as measured by reduced AchE activity is correlated with the symptoms of dementia. Our study used the tracer 1-[^{11}C]Methylpiperidin-4-yl propionate (PMP) to obtain an index of the regional AchE activity by estimation of a model parameter. Prior to model analysis, the best fitting function to correct for metabolites in the plasma was evaluated and appeared to be the Hill function if all samples were included. An accurate input of the two-tissue irreversible compartmental model, the standard model to describe the PMP kinetics, is essential because it controls the output i.e. the model parameters. By comparing the irreversible with the reversible compartmental model, we confirmed the irreversible character of PMP. Moreover, we showed that inclusion of the plasma fraction as an additional parameter improved the model fit when taking the plasma input function that was corrected for metabolites as a measure for the vascular pool in the brain. In addition to compartmental models, the non-invasive alternatives reference method and shape analysis were assessed for their power to describe the kinetics of PMP but poor results were obtained. Furthermore, we explored preliminary the possible role of the cholinergic system in two types of disorders that respectively will and might lead to dementia i.e. primary progressive aphasia and mild cognitive impairment. No differences in AchE activity with healthy controls at baseline were found. Nevertheless we were able to detect changes in the activity of AchE after treatment of both patient groups with galantamine, a cholinesterase inhibitor.

List of abbreviations

^{11}C	Carbon-11
1T1k model	One-tissue one-rate constant model
1T2k model	One-tissue two-rate constant model
2T3k model	Two-tissue three-rate constant model
2T4k model	Two-tissue four-rate constant model
Acetyl coA	Acetyl coenzyme A
Ach	Acetylcholine
AAL	Automatic anatomic labeling
AchE	Acetylcholinesterase
AD	Alzheimer's disease
AIC	Akaiki criteria
AMP	1-[^{11}C]Methylpiperidin-4-yl acetate
BFC	Basal forebrain complex
CDR	Clinical dementia rate
ChAT	Choline acetyltransferase
ChE-I	Cholinesterase inhibitor
CM	Compartmental modeling
COV	Coefficient of variation
FDR	False discovery rate
GM	Grey matter
HACU	High affinity choline uptake
HC	Healthy controls
HPLC	High performance liquid chromatography
L	Left
LOR	Line of response
mAchR	Muscarinic acetylcholine receptors
MBC	Metabolite correction
MCI	Mild cognitive impairment
MNI	Montreal Neurological Institute
MRI	Magnetic resonance imaging
nAchR	Nicotinic acetylcholine receptors
NBM	Nucleus basalis magnocellularis
nbM	Nucleus basalis of Meynert
NLS	Non-linear least squares

PET	Positron emission tomography
PMP	1-[^{11}C]Methylpiperidin-4-yl propionate
PPA	Primary progressive aphasia
REF	Reference method
R	Right
SA	Shape analysis
SC	Schwarz criteria
SD	Standard deviation
TAC	Time-activity curve
VOI	Volume of interest
WM	White matter

Table of contents

1. Introduction

The cholinergic system of the brain is disturbed in several types of dementia. Neuropathology research both postmortem and in vivo has generated substantial evidence for alterations in the cholinergic transmission of dementia patients, especially in the case of Alzheimer's disease (AD). Acetylcholine (Ach) is the neurotransmitter for cholinergic signaling and known to play a pivotal role in memory and learning. Therefore, the link between AD and the cholinergic function evident as it was, has been a major tenet in research for over 30 years. Profound cholinergic cell loss and reduction in markers of the cholinergic synapse have been observed consistently in the brain of AD patients. The loss of cholinergic neurons is not general but selectively present at the basal forebrain complex (1). As the complex signals to the entire cortical mantle and limbic areas, it is not surprising that damage of these cholinergic innervations was suggested to cause dysfunction. And indeed long-standing evidence correlates the cognitive impairment in AD with the observed cholinergic deficit.

The imaging modality positron emission tomography (PET) provided the mean to assess the cholinergic neuronal damage in the living human brain. With the design of PET tracers that target the cholinergic synapse, the possibility popped up to visualize in vivo the integrity of the cholinergic system. Based on a well-established marker of the cholinergic integrity i.e. acetylcholinesterase (AchE), Ach-analogue tracers were developed (2). As AchE is the breakdown enzyme of Ach, also for these tracers the mode of enzyme action involves hydrolysis and is highly specific. This generates a radiolabeled metabolite that accumulates in brain tissue at a rate that is indicative of AchE activity. The tracers 1-[^{11}C]Methylpiperidin-4-yl acetate (AMP) and 1-[^{11}C]Methylpiperidin-4-yl propionate (PMP) are used to study the activity of AchE in the brain of healthy subjects and dementia patients.

The regional distribution of both tracers corresponded well with the distribution of AchE from postmortem studies (3). In addition, using PET and the Ach-analogue tracers, a consistent reduction of AchE activity was observed in the brain of AD patients, which was again in accordance with necropsy data. Even though both tracers are targets of the enzyme AchE, their kinetic properties differ. The hydrolysis rate of PMP is three to four times slower than the AMP tracer and as a consequence delivered more reliable estimates in regions with moderate to high AchE activity (4). Therefore we decided to use the PMP tracer in this study for quantification of AchE activity. An index of the regional AchE activity can be obtained by estimation of a model parameter. Indeed, a proper kinetic model allows extracting from the measured PET signal the parameter of interest i.e. the AchE activity.

The plasma concentration of the intact tracer over time is required as input for the kinetic model. Therefore, we first evaluated the metabolite correction. Following the search for the accurate model input, the second aim of our study was to find the compartmental model that describes best the behavior of PMP in our set of data. Different types of compartmental models were compared, not only to test the irreversible character of the tracer but also to evaluate the added value of the plasma fraction in the model. However, compartmental modeling requires arterial sampling, which is invasive and induces additional variability. Therefore it was interesting to test also the ability of the non-invasive alternatives that are available for the PMP kinetic analysis, which was the third aim of this study.

Next to the regional quantification of AchE either by invasive or non-invasive models, another interesting characteristic of using an Ach-analogue tracer is its ability to monitor the effects of a drug class called cholinesterase inhibitors (ChE-Is). Those therapeutic agents are so far the most effective drugs to treat the symptoms of dementia. However this strategy has only a limited effect and better understanding of the cholinergic system and its role in dementia is needed. Since AD is believed to have an extensive preclinical stage, this feature can be used to further unravel the role of the cholinergic deficit in the etiology of AD pathogenesis. PET imaging offers the advantage to measure in vivo at an early stage, while for most postmortem studies the studied brains were already in an advanced stage of the disease.

The problem of using PET as a tool to detect patients who will develop dementia is to find a target population that does not yet have dementia but is already presented in a clinical setting due to the presence of symptoms. Therefore, the final aim of the study was to study preliminary the activity of AchE in both MCI and PPA patients, before and after treatment with the ChE-I galantamine. Patients with mild cognitive impairment (MCI) are thought to be a prodromal stage of AD. MCI is a clinical condition in which memory is mildly impaired by definition but the global cognitive function and daily life activity are intact (5). Patients with this disorder are at high risk to develop dementia (6). However, some will develop dementia whereas others will not. This is in contrast for patients with primary progressive aphasia (PPA), which is a disorder characterized by an onset of dominant language disability caused by selective neurodegeneration (7). These patients will eventually, in a later stage, all develop dementia.

For both disorders no effective drug is available. Quantification of AchE activity by in vivo PET imaging might assess whether or not changes in the activity of this cholinergic marker are present, as compared to healthy controls. Indeed, besides investigating the cholinergic system with regard to dementia also the effect of the medicinal treatment for dementia i.e. ChE-Is can be monitored using PET, a suitable tracer and kinetic model.

2. Literature study

2.1 The cholinergic system and dementia

Degeneration of cholinergic neurons in the brain is characteristic for a number of dementia-related disorders. The type of dementia that was investigated most extensively regarding the link with cholinergic transmission is Alzheimer's disease (AD). A large body of evidence over more than 30 years and from both ante- and postmortem studies consistently showed damage to the cholinergic pathways originating from the basal forebrain. The relation of this cholinergic deficit with cognitive dysfunction led to the development of the cholinergic hypothesis, which states that the loss in cholinergic function significantly contributes to the symptoms associated with AD. Later on it formed the basis for the development of a class of drugs called cholinesterase inhibitors (ChE-Is). To date these agents represent the most effective treatment to alleviate the symptoms of dementia, albeit with a rather moderate benefit.

2.1.1 Central cholinergic system

The cholinergic system, which is present both central and peripheral, can simply be defined as the system that uses acetylcholine (Ach) to mediate signaling (8). In the brain, two main types of Ach-utilizing neurons exist: the projection neurons and the interneurons (9, 10). Cholinergic interneurons are predominantly present in the striatum whereas the projection neurons are mainly localized in the upper brain stem and the basal forebrain complex (BFC). This complex contains a network of cholinergic cell bodies scattered among four nuclei: the medial septal nucleus, the vertical and horizontal nucleus of the diagonal band of Broca and the nucleus basalis of Meynert (nbM) (11-13).

Each nucleus projects to a different neuroanatomical target (9, 14). The hippocampus is mainly innervated by the medial septal nucleus, whereas the anterior cingulate cortex and olfactory bulb are innervated by respectively the cholinergic neurons of the vertical and horizontal nucleus of the diagonal band of Broca. The last nucleus is the nbM, which provides cholinergic innervation to the rest of the cortex, including limbic structures such as the amygdala and hippocampus (13).

Thus, the entire cortex receives cholinergic input that originates from the BFC. Therefore cholinergic transmission in the brain is one of the most important neuromodulating systems. Nearly all cognitive functions but especially learning, memory and attention rely for a significant part on the BFC (15, 16).

2.1.2 Acetylcholine synthesis and breakdown

The signaling molecule of the cholinergic system is Ach, a neurotransmitter with a variety of functions. The multiple roles of this small molecule are widely discussed, particularly the function of Ach in learning and memory (17-19). Ach is peripherally the neurotransmitter at neuromuscular junctions and at synapses in the ganglia of the autonomous nervous system; centrally it is a modulator at a variety of sites within the central nervous system (20).

The synthesis of Ach is a one-step reaction catalyzed by the enzyme choline acetyltransferase (ChAT) (8, 10, 20). This enzyme synthesizes Ach from two building blocks: choline and acetyl coenzyme A (acetyl coA). Synthesis takes places in the cytosol of the nerve ending by transferring an acetyl group from acetyl coA to the second precursor choline. First Ach is manufactured; secondly it is transported and packaged into synaptic vesicles by the vesicular Ach transporter. After packaging, Ach is stored at the nerve ending until an action potential arrives and allows for its release into the synaptic cleft.

At the postsynaptic site, Ach can interact with two types of cholinergic receptors: the muscarinic- and nicotinic Ach receptors (mAchR, nAchR) (8, 10, 21). The family of nAchR signals via ligand-gated ion channels and is characterized ionotropic (22, 23). The mAchR are part of the superfamily of membrane-bound G protein-coupled receptors and therefore metabotropic (24). Both the mAchR and nAchR are located at the pre- and postsynaptic membrane to mediate signal transduction (8). After binding of the Ach neurotransmitter to its receptors, the enzyme acetylcholinesterase (AchE) will terminate cholinergic transmission (8). By hydrolyzing Ach into choline and acetic acid, this catalyzing enzyme terminates the synaptic action of Ach. The breakdown of Ach allows choline to return to the presynaptic terminal, where it can be reused for further Ach assembling. A high affinity choline uptake (HACU) transporter, energy dependent and present at the pre-cholinergic nerve ending, pumps the extracellular choline back inside the nerve button.

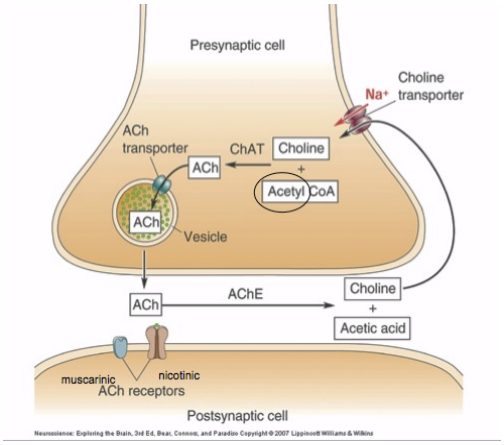

Figure 2.1 The cholinergic synapse. Abbreviations: Ach= acetylcholine; ChAT= choline acetyltransferase; AchE= acetylcholinesterase; acetyl coA=acetyl coenzyme A (25).

2.1.3 AchE and the cholinergic hypothesis of Alzheimer

AchE is the regulator of Ach concentration at the synapse of the cholinergic system (26). It is one of the fastest enzymes in the body that belongs to the family of cholinesterases, a class of serine hydrolases (27). The enzyme acts by hydrolyzing Ach into its two building blocks, achieving thereby the termination of Ach signaling. AchE is present in a soluble form at the synaptic cleft and in a membrane-bound form at both the membrane of pre- and postsynaptic neurons of the cholinergic system (28). As AchE is an essential component of the cholinergic synapse, it was one of the important players in the mapping of the cholinergic system. Indeed the neurons and trajectories of the central cholinergic system have been discovered by in vitro measurements of cholinergic markers using immunohistochemistry and in-situ hybridization methods (29-31). Other markers included additional compounds of the synapse i.e. ChAT, vesicular Ach transporter and nAchR/mAchR (29, 32).

In the late 1970s, growing interest in the cholinergic system aroused by the discovery that brain biopsies displayed significant and selective reduction of Ach-related enzymes (1, 33-35). Markers such as AchE and ChAT were reduced in the cortex and hippocampus of AD patients (1, 34-37). Whitehouse et al.[36] confirmed the cholinergic deficit by observing degeneration of cholinergic neurons at the nbM in postmortem AD brain, thereby explaining this loss of cholinergic markers. Next, the observed association between the cognitive decline in dementia and the cholinergic lesion encouraged the relevance of the relation between AD and the cholinergic dysfunction (38). So a large body of evidence eventually provided the cholinergic hypothesis to be formulated. This hypothesis states that the cognitive deficit in AD is correlated with a disrupted cholinergic transmission (39, 40).

Based upon the cholinergic hypothesis, further research on the cholinergic link with cognitive impairment (especially dementia) was stimulated. Several approaches arose to design drugs that improve the cholinergic function (41, 42). Up to now, among the drugs that target the cholinergic transmission, solely the class of the ChE-Is has been effective in treating the symptoms of AD (43). The treatment with ChE-Is is based upon stimulation of the cholinergic function. Inhibition of the enzyme AchE delays the breakdown of Ach and thus prolongs signaling of this neurotransmitter. Substantial evidence in patients with mild to moderate AD showed temporal increase or stabilization of cognitive and global functioning after treatment with ChE-Is (44). The improvements induced by these agents are considered rather small but with statistical significance (45). The efficiency of ChE-Is supported the cholinergic hypothesis and encouraged the role of AchE in AD research (46, 47). Currently four types of ChE-Is are approved and in use in most countries: donepezil, galantamine, rivastigmine and tacrine (48). All four types have proven to alleviate the symptoms of AD but are unable to

cure the disease (42). Furthermore the response to a specific type of ChE-I is variable. Indeed, not all patients have beneficial effects after intake of ChE-Is such that dementia patients are divided in responders and non-responders (49). A method defining early on good response to a type of ChE-I would facilitate the choice of agent for symptomatic treatment of dementia.

2.1.4 MCI and PPA: is there a cholinergic link?

Dementia is an umbrella term referring to a clinical syndrome that is characterized by a decline in memory or other cognitive functions affecting a person's ability to perform daily life activities (50). The cause of dementia is degeneration of neurons in the brain, which leads to malfunctioning and changes in multiple cognitive systems (51). Since neurodegeneration starts many years before onset of clinical symptoms, diagnosis at an early stage is challenging (52).

AD, the most common form of dementia accounting for an estimated 60% to 80% of all cases, is characterized by an insidious onset of memory impairment and progressive cognitive deterioration (51). At a more advanced stage of the disease, emergence of neuropsychiatric manifestations and basic functional decline develops (50). The first hypothesis ever about the etiology of AD was the cholinergic hypothesis (see above) (39). However, a shift took place towards the typical AD hallmarks like amyloid plaques and neurofibrillary tangles. This perhaps because of the moderate effect of the ChE-Is that is purely symptomatic and does not cure AD, but probably also because later studies observed that cholinergic enzymes were not reduced in the early stages of AD (53). It is still inconclusive whether or not cholinergic degeneration is an initial stage of AD. In case the neuropathology of a changed cholinergic function would precede the clinical manifestations of dementia, then a biomarker that predicts outcome in a non-demented but preclinical group could be developed.

According to the criteria and guidelines of the National Institute and Health in 2011, AD has three main stages: preclinical AD, mild cognitive impairment (MCI) due to AD, and dementia due to AD (52, 54). MCI refers to a condition in which memory loss and/or other cognitive dysfunctions are present more than would be expected from normal aging but not to an extent that it significantly interferes with daily functioning (5). Individuals suffering from MCI do not yet have dementia but have a high risk developing it (6, 55). However, not all MCI patients will develop AD or any other type of dementia (6, 51). Clinical subtypes of MCI patients that likely differ in their ultimate fate were identified (6, 56). They can be classified into amnestic MCI and non-amnestic MCI, which refers respectively to the involvement of a

memory complaint or not. Next, impairment in only one or multiple cognitive domains is investigated to categorize further into single- or multiple domain MCI respectively (56, 57).

Some MCI patients develop dementia, whereas others don't and even might improve or stabilize after a period of time (6, 51). The progression rate from MCI to dementia is between 16% and 50% and this over a period of 3 years (5). As a consequence, numerous randomized clinical trials with ChE-Is were performed in MCI patients. ChE-Is, the drug class used in mild to moderate AD, was hypothesized to alleviate the symptoms of MCI and even delay possible progression to dementia. But several meta-analyses did not found benefit of ChE-I therapy in MCI patients (58-60). Despite the consistent negative results of ChE-Is, it is still indecisive whether or not treatment should start in a subtype MCI stage. Therefore, homogenous group analyses with one clinical MCI subtype and more standardized diagnostic criteria are needed (58). As MCI patients are at increased risk to develop dementia, with one subtype having more risk than another, it is considered a useful clinical stage in which early intervention might be beneficial (61, 56). In addition to the study of ChE-Is in MCI patients, pathological brain features were examined using neuroimaging to predict MCI patients that will progress to dementia (61).

In contrast to MCI, primary progressive aphasia (PPA) is a disorder with a certain progression towards dementia. PPA is a heterogeneous clinical syndrome in which predominantly the language network is affected by selective degeneration of the language–dominant brain areas (7, 62, 63). Depending on the anatomical distribution of cortical atrophy, the language disorder can take the form of aggramatic, logopenic or semantic aphasia (7). Those are the three main variants of PPA, which differ in their pattern of language deficit (64, 65). As the condition progresses, other (i.e. non-verbal) cognitive functions start to decline and in the final stage the patients suffer from dementia. Sometimes the PPA disorder is even considered having the same three-stage framework as AD (66, 67). Until now, no drug treatment is available for this group of patients. Therefore development of an effective PPA medicinal therapy is of importance for this disorder that has a large impact on daily life functioning.

Few studies investigated specifically the cholinergic system in those two patient groups, MCI that is considered a pre-phase to dementia and PPA that will develop to dementia in any case (68). In vivo PET studies quantifying the activity of AchE can shed light on the early role of the cholinergic system in dementia. In addition, ChE-Is can be evaluated for their possible benefit and effect in patients that not yet have an effective drug available.

2.2 Dynamic brain-PET of AchE activity

2.2.1 Positron emission tomography

PET stands for positron emission tomography. It is a functional imaging modality that makes use of an imaging device, the PET scan and an imaging agent, the tracer molecule. The PET process starts with the production and choice of an appropriate tracer followed by administration to the subject, usually by intravenous injection. The PET scan, in which the subject was placed, will then detect the emitted radioactive signal (69). Indeed, the tracer is composed of an unstable short-lived radioisotope attached to the molecule of interest. The radionuclides used for PET decay by positron emission to achieve more stability (70). After radioactive decay, the positron travels a minimum distance through body tissue until annihilation takes place, which is the interaction of the emitted positron with an electron of the surrounding tissue. At annihilation, the mass of the particles is converted into energy under the form of two photons. Both have energy of 511 keV and are emitted in opposite direction (~180° apart). Next, the pair of photons is detected in coincidence by opposing detectors. As annihilation takes place within a very short time period (~10^{-9} ms) and only a few millimeters away from the emission site, it provides a good indication of the tracer's location inside the body (71).

The process of annihilation offers not only the basic principle of PET but also delivers the properties favorable for imaging. At first, the specified level of energy (511 keV) allows designing a scanner with high specificity. Secondly, the photons are highly energetic such that the chance the photons can escape the body and reach the detector is high. And third, the back-to-back photon emission creates a line connecting the two detectors that measured the two photons. This line is called the line of response (LOR) and contains the site of annihilation. Since the annihilation photons are simultaneously created, it is a coincidence event. Millions of events will eventually provide information about the tracer concentration and distribution within the human body. Figure 2.2 illustrates in a nutshell the basic principle of PET.

A PET scan makes use of a scintillator to detect the photons (69, 70). This gamma-ray detector consists of dense crystalline material that has high probability to catch the photons, mainly by photoelectric absorption. In this interaction, the detector absorbs all of the photon's energy and subsequently emits a photoelectron. This particle will pass trough the crystal by distributing its energy to the electrons, which on their turn will emit light in the visible spectrum. Subsequently, a photomultiplier tube detects these optical photons and converts the light signal into an electric current.

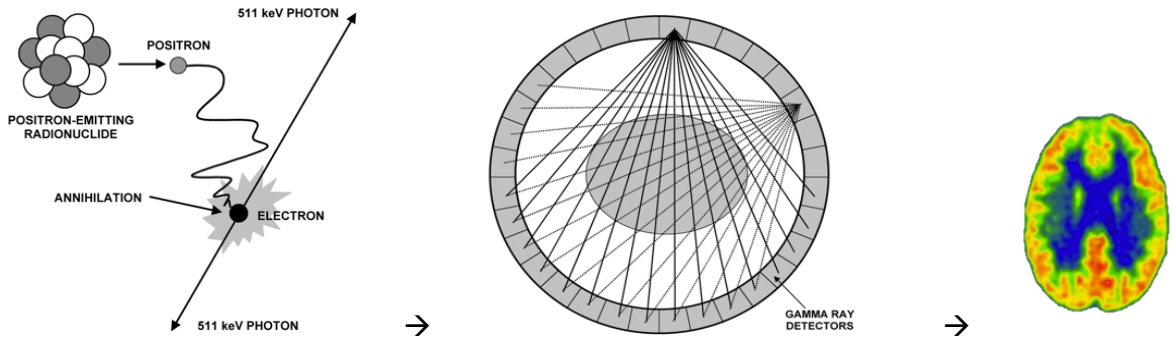

Figure 2.2 The basic principle of PET imaging. After decay of the short-life radionuclide from the tracer, a positron is emitted. This particle will interact with an electron of the body part scanned. Here, an annihilation event takes place that will emit two photons with the same energy of 511 keV in opposite direction. The line these photons create, allow the opposed detectors to track the origin of annihilation. Finally, all the detected events will be reconstructed into a PET image (70).

Once the data are acquired, a last step in the data collection involves the storage of the data in the computer. The raw data, which enclose the coincidence events, are represented in sinograms or in list mode. A sinogram is a 2D-matrix in which each element signifies the number of events recorded along a LOR, defined by a detector pair (70). The storage in sinograms is done for each time frame, which needs to be specified as part of the acquisition. In list mode, each single event is stored separately in terms of the precise timing of the event and the corresponding detector pair. The procedure requires a rebinning of the data in frames, which can be specified after the acquisition.

Next, the reconstruction into a 3D-image can start after several corrections for physical effects such as radioactive decay, attenuation, scatter and random events. The raw data i.e. the detection of the annihilation photon pairs need to be reconstructed into images that quantitatively represent the tracer distribution. By summing up all photon pairs emitted along a certain LOR during a specified time period, the line integral of the emitted radioactivity along that line is attained (72). If a set of these line integrals that all have the same angular directions is considered, the parallel projection of the tracer distribution at that specified angle is obtained. Image reconstruction of PET data converts different line integrals at many different angles around the subject into a 3D-image using either filtered back projection or an iterative algorithm (70). The output of the reconstruction process is a 3D-image where the signal intensity of each voxel or volume is proportional to the local tracer concentration. A calibration factor will finally convert the radioactive signal into a local tracer concentration.

In general one wants to measure the tissue concentration of the tracer as a function of time. This implies dynamic PET scanning. Therefore not a single scan but multiple scans (so-called frames) are acquired. The time sequence of PET data allows measurement of the cerebral uptake and clearance of the tracer over a pre-specified period of time (73).

Depending on the half-life of the tracer this period ranges from the start of injection up to 30-60 min (sometimes 120 min and more) after injection.

Dynamic brain-PET data represent the tracer distribution in cerebral tissue at specific time points. Regional tracer radioactivity as a function of time is called the time-activity curve (TAC), which can be measured both on the level of a voxel or volume. Additional use of a kinetic model offers the ability to translate the PET data into the quantification of a biological process that the tracer specifically targets. Thus, the combination of dynamic brain-PET data with kinetic modeling enables the in vivo measurement of neurobiological systems and functions.

2.2.2 Compartmental modeling

The most commonly used model to describe the kinetics of the tracer within a physiological system is the method of compartmental modeling (CM) (69, 74). This method simplifies the biological system of interest by use of distinct compartments. Each compartment represents a possible state of the tracer, which can be either an anatomical location (extravascular space, intercellular space…) or a chemical form (metabolite, protein-bound…) within the system targeted by the tracer. Exchange between the different compartments is defined by rate constants. Those parameters are estimated by solving the mathematical representation of the model.

To illustrate the basic principles of CM, a one-tissue two-rate constant (1T2k) model will be shortly described. The 1T2k model is the simplest model since only a single compartment in the tissue is defined. This model is characterized by two compartments (the arterial blood and the tissue compartment) and two first-order kinetic rate constants, K_1 and k_2, as depicted in figure 2.3.

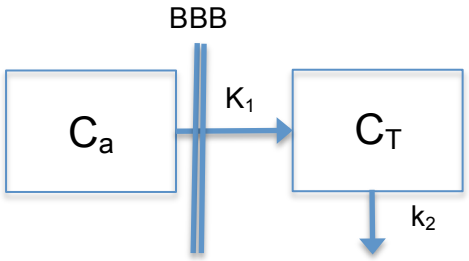

Figure 2.3 Schematic representation of a one- tissue two-rate constant model. This model has only a single compartment in tissue. From the arterial blood compartment C_a, which represents the authentic tracer concentration in the blood, the tracer flows to the tissue compartment. The tracer concentration C_T in the tissue compartment receives input from the arterial blood space at a rate constant defined by K_1. The other rate constant k_2 determines the rate of concentration loss from C_T. BBB= blood brain barrier.

The parameters K_1 (mL/min·g) and k_2 (min^{-1}) designate the rate constants for influx to and efflux from tissue, respectively. $C_a(t)$ represents the time-varying tracer concentration present in the arterial blood, as measured by arterial sampling (see further). $C_T(t)$ on the other hand is the time-varying radioactivity concentration that is measured in a given tissue region.

To describe the tracer influx and efflux from each tissue compartment over time, differential equations are used (69). The differential equation allows describing mathematically that the rate at which concentration changes over time within a tissue compartment depends on the concentration entering and exiting (75). Since the 1T2k model has only one tissue compartment, a single differential equation explains the model. The change of tracer concentration over time within the tissue compartment C_T is described by the following mathematical equation:

$$\frac{dC_T(t)}{dt} = K_1 C_a(t) - k_2 C_T(t)$$

where the influx from the blood to tissue is the factor K_1C_a and k_2C_T represents the efflux from the tissue to blood. C_T and C_a are respectively tissue and arterial blood concentrations as function of time t,

The equation can be solved for C_T. An explanation about mathematical techniques for derivation is beyond the scope of this manuscript, a textbook on linear differential equation can be consulted, e.g. (76). The general solution for C_T as a function of time (74):

$$C_T(t) = K_1 e^{-k_2 t} \otimes C_a$$

The symbol ⊗ is the convolution operator.

The total radioactive signal measured by PET represents the tracer uptake in a volume of interest (VOI) or a voxel, depending on the level of analysis. Since next to tissue radioactivity also intravascular activity contributes to the total signal, this factor should be taken into account. Consequently, the total tracer concentration measured by the PET scanner is given by:

$$C_{tot}(t) = C_T(t) + V_b C_a(t)$$

where C_{tot} is the total radioactive concentration measured in the brain by PET, C_T is the total tissue concentration and V_b is the fraction of measured volume occupied by blood. C_a defines the arterial whole blood concentration as a function of time, either corrected or uncorrected for metabolites in the brain. The solution of C_{tot} is fitted by a least square optimization method

to the regional brain TAC, with as input the metabolite-corrected plasma TAC. The aim of the fitting is to find estimates for the rate constants K_1 and k_2 that explain best the measured data (77).

The input of the model is delivered by the arterial sampling during the PET scan session. The direct measurement of blood samples provides the whole blood TAC i.e. the concentration of the radiotracer in the whole blood as a function of time. Since it is the concentration of the parent fraction in plasma that is required for data quantification, the measured whole blood radioactivity needs to be corrected for the whole blood to plasma ratio, and metabolites. For metabolite correction (MBC), additional blood samples are taken throughout the PET scan session. Subsequently, the fraction of metabolized tracer in the plasma can be assessed using high performance liquid chromatography (HPLC). Though, the number of blood samples is restricted due to practical and technical reasons. Additionally, the estimations of the metabolite fraction by HPLC might be unreliable towards the end of the scan session. As a consequence a fitting function is needed to enable the full time course of the "true" radioactivity i.e. the radioactive signal of the authentic tracer fraction in plasma.

The metabolite-corrected plasma curve as a function of time is obtained in two steps 1) the total plasma curve is acquired by fitting the ratio of plasma to whole blood with a multi-exponential model and 2) the total plasma curve is multiplied with a fitting function to obtain the plasma curve corrected for metabolites. The authentic tracer fraction (so-called parent fraction) is then the input of the kinetic model. To exemplify this procedure, the MBC of the plasma input function with the Hill function as fitting function will be displayed for the tracer 1-[^{11}C]Methylpiperidin-4-yl propionate (figure 2.4 and 2.5), as this tracer will be discussed more profoundly later on.

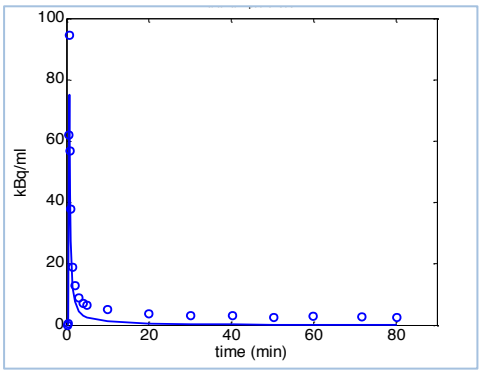

Figure 2.4 Arterial input function over time. The dots represent the measured total tracer radioactivity in plasma including both authentic tracer and metabolites. The full line designates the metabolite-corrected plasma.

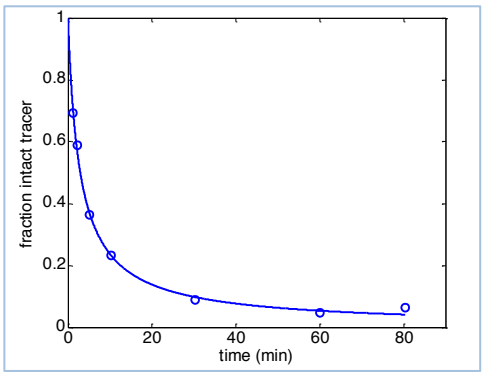

Figure 2.5. **Fraction of the intact tracer over time, fitted by the Hill function.** The fraction dropped to below 50% by 5 min, and after 30 min below 10% was left. Dots represent the measured intact tracer fraction, the full line designates the fit.

To recapitulate, a compartmental model is a mathematical model. The PET data and the arterial plasma input are known data that are measured. The unknown parameters of the model are the rate constants and/or whole blood volume fraction. Those need to be estimated by fitting the measured PET data to the theoretical function with as input the metabolite-corrected plasma TAC.

The choice of the model configuration for CM depends upon the radiotracer. In other words, the chemical and biological characteristics of the tracer determine the number of compartments in the model. For example, the one- tissue model is mostly used in blood flow measurements with as PET tracer oxygen-15 labeled water. The kinetics of this tracer is only determined by the tracer flow, not by changes in metabolism. On the contrary, for receptor-binding or metabolism studies, the binding of the tracer to the receptor or metabolizing enzyme influences the tracer's kinetics (75, 78, 79). Therefore, in binding studies not a one-tissue but a two-tissue model is often used. In the latter, the second tissue compartment represents the bound concentration of the tracer, as depicted in figure 2.6.

By adding a second compartment in the tissue, extra rate constants named k_3 and/or k_4 need to be defined but the latter only in case of reversible binding. Indeed, depending on the tracer targeting a specific system under investigation, binding might be reversible or irreversible. The parameter k_3 defines the rate at which the tracer binds the receptor or enzyme, whereas k_4 is the rate constant for reversible binding and efflux or de-metabolisation of the metabolites.

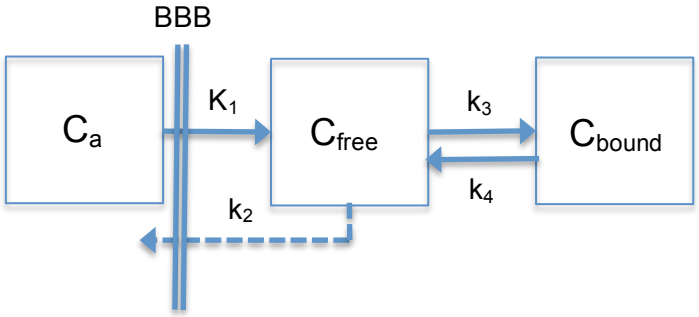

Figure 2.6 Schematic representation of a two-tissue four-rate constant model for binding studies. K_1 is the rate constant that defines the transport across the blood brain barrier (BBB) from the arterial blood compartment (C_a) towards the brain tissue compartment with free tracer concentration (C_{free}), whereas k_2 represents the efflux of free tracer. The rate of free tracer binding is represented by k_3. After binding, the tracer can either stay in the tissue compartment with metabolized tracer (C_{bound}) concentration or it can be transported back to C_{free} at a rate represented by k_4.

As stated before, a compartment designates a possible state of the tracer, which is either a space or a chemical state. The change in local concentrations within the compartments is considered being regulated by the tracer transport and/or –binding, which are possible states of a tracer. Estimation of the rate constants then provides information about the rate of tracer transport and/or binding. Important to note is that for receptor-binding studies the non-

specific binding and the free tracer are considered as one compartment. If not, the model would become too complex being composed of six rate constants.

To finish the topic about CM, it must be mentioned that general assumptions underlie the use of a PET tracer model. One assumes that the model parameters are constant over time (74). This implies the kinetic parameters to be studied in a physiological system that is in steady state, at least during the PET scan session. Additionally it is required that the compartments are homogenous in concentration.

2.2.3 Previous PET studies for quantification of AchE activity

Before PET imaging of AchE was established, appropriate radiopharmaceuticals that target the enzyme were developed. Irie et al.[2] introduced the concept to measure AchE activity in vivo with Ach-analogues. This research group first designed and secondly evaluated in mice a set of methylated piperidyl esters that were radioactively labeled with carbon-11 (^{11}C). The tracers were developed to have the following features: 1) lipophilic enough to cross the blood brain barrier, 2) the compounds should be molecular similar to Ach to allow high specificity for AchE and 3) once hydrolyzed by AchE, they should become hydrophilic and get trapped inside the brain tissue such that transport back into the vascular system is no longer possible. Of the whole set of piperidyl esters, 1-[^{11}C]Methylpiperidin-4-yl acetate (AMP) and 1-[^{11}C]Methylpiperidin-4-yl propionate (PMP) were selected for further evaluation in PET studies.

Previous to tracer application in humans, a full examination in animal models was needed. Kilbourn et al.[80] studied in mice the in vivo metabolism of AchE. The results indicated the rapid diffusion of both tracers into the brain and a consistency of regional cerebral distribution with in vitro studies. In addition, significant differences between both esters were discovered. The PMP tracer delivered better discrimination between cortex and striatum than AMP but at all brain regions, except the striatum, the radioactivity concentration was higher for AMP than for PMP. Not only a mouse model was studied, Kilbourn et al.[80] also performed a PET imaging study with a female pigtail monkey. Here a remarkable difference between both piperidyl esters was observed in both the shape of the TAC and the relative amount of tracer trapped in the cortex and striatum of this primate brain. AMP showed faster tracer uptake with negligible efflux from striatum and cortex, whereas PMP showed a high initial uptake but with a significant washout the first 15 min, about 15% striatal and 50% cortical washout. Again, as observed in the mouse model, the PMP tracer had significantly greater power to distinguish between the brain regions cortex and striatum than AMP. Irie et al.[81] executed additional studies in rats with unilateral an induced AchE hypofunction at the nucleus basalis magnocellularis (NBM) to confirm the tracer sensitivity to AchE activity that was suggested in

their earlier paper (2). This type of lesion resulted in a selective reduction of cerebral cholinergic markers. Since the NBM is one of the major providers of cholinergic innervation to the neocortex and the rat NBM is homologous to nbM in human brains, a good animal model to study the relationship between the tracer and the AchE activity in a disrupted cholinergic system was created.

Eventually, Iyo and colleagues[3] made the step to humans. This study with eight healthy subjects and five mild AD patients showed that PET imaging with AMP could be used to measure AchE activity in vivo. The distribution visualized by PET correlated well with the AchE distribution at necropsy, except for the striatum. In the AD patients, significant reduction of AchE activity was found in cortical regions. These findings were further confirmed two years later by a second PET study with AMP (82). Here, they additionally investigated the effect of age on AchE activity at the cortex, but no correlation was observed. Next to AMP, the PMP tracer was evaluated in humans. Kuhl and colleagues[83] demonstrated that also the distribution of PMP was in accordance with the distribution of AchE studied postmortem. At the same time, this research group showed with simulations studies that AchE activity estimated by k_3 did not depend on the blood flow, which was in accordance with the study of Namba et al.[82]. In addition, the lack of correlation between k_3 and age observed previously was confirmed in this study (82, 83). The effect of gender on the estimation of k_3 showed no relation as well (83).

In the same year, Koeppe et al.[4] confirmed the validity of PMP to map the distribution and activity of AchE. Indeed, PMP trapping in the brain depends upon both the regional level and action of the enzyme AchE. As a consequence, this tracer provides information about the functional aspect of AchE instead of just its distribution (84). Furthermore, this group took a next step in the kinetic analysis of PMP by evaluating four distinct approaches for parameter estimation. They concluded that all four alternative analyses provided an extremely precise estimate for the index of AchE activity (alias k_3) in regions with low to moderate enzyme activity. On the other hand, in regions with high activity such as the striatum and cerebellum, the estimates for the action of AchE were much less precise.

Later studies on the in vivo measurement of AchE all confirmed the ability of both tracers AMP and PMP to visualize the enzyme distribution, to quantify its activity and to detect reduction in AD patients (85-88). In addition to the standard tracer model, in these studies non-invasive models (see further) to provide reliable estimates for the model parameter k_3 without the need of arterial sampling were developed. Overall the conclusion was that non-invasive models were nearly as effective as the standard invasive method to identify cortical regions with significant reduction in the brain of AD patients.

2.2.4 Kinetic models for AchE

The cholinergic system has been studied in vivo by the use of brain-PET. This imaging technique mapped the biological function of AchE using as radiotracer either AMP or PMP, which are both Ach-analogues. Combining dynamic PET data with a proper kinetic model for the tracer allows in vivo quantification of Ach hydrolysis in the human brain.

To perform appropriate modeling of the AMP/PMP tracer kinetics, a two-tissue three-rate constant (2T3k) model is generally used (89), as displayed in figure 2.7. The brain tissue contains two compartments representing the authentic tracer and its metabolite. The third compartment is referred to as the arterial blood compartment. The tracer can flow between all three compartments and the rate of exchange is designated by three rate constants. The transport between the arterial blood and the brain tissue is represented by K_1 and k_2, whereas k_3 designates the transport between the two brain tissue compartments (figure 2.7).

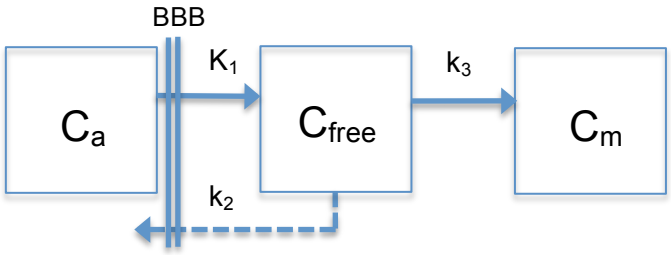

Figure 2.7. **Schematic representation of the two-tissue three-rate constant model for AMP and PMP**. K_1 is the rate constant that defines the transport across the blood brain barrier (BBB) from the arterial blood compartment (C_a) towards the brain compartment with authentic tracer concentration (C_{free}) whereas k_2 represents the efflux of the unmetabolized tracer. The rate of hydrolysis of the authentic tracer is represented by k_3. After hydrolysis, the metabolite gets trapped in the brain tissue compartment with the concentration of the metabolized tracer (C_m).

The rate constant K_1 (mL/min·g) defines the rate of tracer penetration into the brain across the blood brain barrier, whereas the rate of k_2 (min^{-1}) is the efflux from the brain back into the arterial compartment in the 2T3k model. Parameter k_3 (min^{-1}) describes the rate of tracer hydrolysis by AchE. Once hydrolysis took place, the metabolite gets trapped at the site of the enzymatic reaction and is assumed to no longer diffuse in between the compartments.

The 2T3k model is the standard model to get a reliable estimate of the clinical relevant rate constant k_3, which is the index of Ach hydrolysis. Since arterial sampling is needed to obtain the input function of this compartmental model, clinical routine application is impeded. Not only a team with substantial expertise is needed, it is also unpleasant to the subject, increases the risk of complications and induces variability and errors related to the plasma activity detection. Therefore, alternatives to this model have been developed such that arterial sampling is no longer required (85, 90). For an irreversible tracer with the

characteristic to get trapped after metabolisation, there are two options available to perform a non-input analysis: the reference method (REF) and the shape analysis (SA).

The REF uses a reference region with a very high activity of AchE. Brain regions like the striatum or the cerebellum are used as a reference since every tracer in these brain structures will get trapped due to the very high activity of AchE. Three types of REF analyses are available (85, 90-91). Herholz et al.[90] developed the analysis whereby the ratio of the target tissue radioactivity relative to the reference tissue radioactivity is taken to exclude the need of arterial sampling. The approach by Nagatsuka et al.[85] on the other hand, proposed to represent the input function in de form of a single integral. Where the Nagatsuka method has only one assumption, which states that the k_3 value needs to be markedly greater than k_2, the Herholz analysis contains a second assumption postulating that the input function has a mono-exponential decline. Zundorf and colleagues[91] extended and modified the technique of Herholz such that the unnecessary approximation (i.e. the input function is mono-exponential) could be eliminated.

The second alternative method without the need of an input function, neither via arterial sampling nor via a reference region, is termed SA (4). The name yet explains the underlying method: the shape of the cerebral TAC delivers a direct estimation of k_3. The SA is applicable to the irreversible tracer Ach-analogues (i.e. AMP and PMP) and is based on four assumptions. The first assumption includes both an initial and final condition. It states that no metabolic tracer product might be present at the time of the first scan whereas at the time of the final scan, no authentic tracer might be left inside the brain tissue. The second assumption requires all tracer metabolites in the brain to be trapped completely at the end of the PET scan session. Since the tracers used in the kinetic model of AchE hydrolysis are considered to be irreversible, this assumption should be satisfied if at least the PET scan time is not too short.

The third assumption is about the total radioactivity in the brain target tissue. The sum of the authentic tracer tissue- and metabolite tissue concentrations must represent the total cerebral radioactivity. As a consequence, the contribution of the vascular pool to the total PET radioactive signal is neglected. The fourth and last assumption to satisfy for the SA to be valid includes the requirement that the amount of concentration in a scan frame depends on the amount of substrate in the previous scan frame, its frame duration and enzyme activity. This assumption will only be valid in case the scan frame duration is short enough such that concentration has not changed too much within one scan frame.

Thus for the Ach-analogue tracers AMP and PMP, both invasive and non-invasive models have been developed. All three the models (2T3k, REF and SA) have shown to provide reliable estimates in regions with low to moderate AchE activity. However, for regions with high hydrolysis, the estimates for k_3 were consistently less accurate.

3. Experimental work

3.1 Material and methods

3.1.1 Subjects

Three groups of subjects were enrolled in the study: two patients groups i.e. primary progressive aphasia (PPA) and mild cognitive impairment (MCI), and a group of healthy controls (HC). In total 30 subjects were eligible for this retrospective study with the inclusion criterion that both a magnetic resonance imaging (MRI) scan and a positron emission tomography (PET) scan are required. One subject was excluded from the analysis due to excess movement. This resulted in a total of 29 subjects (67.0 ± 1.2 years; mean age ± standard deviation (SD)) with the following division: nine HC, eight MCI patients and 12 PPA patients. In the group of HC (range 59.7 to 76.6 years) with an age average of 65.6 years, all subjects had a clinical dementia rate (CDR) of 0. For the PPA patients (range 52.5 to 78.6 years), the CDR scores had an average of 1 and 68.0 years was the average age. All patients in the MCI group (range 55.1 to 74.9 years) had a CDR score of 0.5 and the average age was 66.4 years.

Detailed neuropsychological examination confirmed the presence of an isolated episodic memory deficit in all MCI patients, according to the Peterson criteria (57). Cerebral abnormalities were checked for and found to be absent in all study subjects. From baseline onwards the subjects were naive for cholinesterase inhibitors (ChE-Is) or antidepressants. For 13 patients (four MCI; nine PPA) the change in AchE activity after intake of the ChE-I galantamine (Razadyne® ER, manufactured by Ortho-McNeil Neurologics) was investigated. This subset of patients had two scans available i.e. baseline and follow-up scan and were taking the drug treatment up to the follow-up scan. The second PET scan of these patients was performed after a period of 1 year (MCI: 366 ± 63 days; PPA: 376 ± 59 days). From the group of HC, five subjects had a second PET scan. These repeat scans were performed after two years (727 ± 72 days), which allowed evaluating test-retest after a two-year interval. So in total 47 PET scans were acquired of which 18 scans were follow-up scans. For a general overview of the characteristics per group, please consult table S-I in the supplementary material. All subjects and/or family members gave their written informed consent in agreement with the declaration of Helsinki. The Ethical Committee of University Hospital Gasthuisberg Leuven approved the study protocol.

3.1.2 Image acquisition protocol

PMP was synthetized according to the methods of Snyder et al.(92). 300 MBq of tracer was injected intravenously as a bolus into the right cubital vein. Prior to tracer injection, a 10-min transmission scan using a gallium-68/germanium-68 rod source was performed. At tracer injection, a sequence of 20 scan time frames (4 x 15 s, 4 x 1 min, 2 x 2.5 min, 10 x 5 min) was acquired over 60 min using a Siemens/ECAT EXACT HR+ PET scanner (Manufactured by CTI PET System, Inc., Knoxville, TN 37932, USA). Measured attenuation correction was performed for all images. For image reconstruction, the scanner software performed filtered back projection using a Hanning filter with cutoff frequency of 0.5. In addition to a PET scan, each subject underwent a high-resolution 3D T1-weighted MRI scan on a 1.5T MRI scanner to obtain anatomical information.

3.1.3 Image processing

Distinct pre-processing steps were applied before the kinetic analysis was executed. For each subject, a sum image of the first eight PET frames was created, representing the average distribution of tracer during the first 5 min post-injection. The remaining 12 scans of each subject were realigned to the individual sum image. Movement was checked using in-house software with the following acceptable upper limits: 2 mm displacement between two consecutive frames, 6 mm translation and 3° rotation across the duration of the scan. Subjects with too much movement were removed from the analysis.

The sum image was co-registered to the subject's MRI with the mutual information algorithm using the SPM 8 software (Statistical Parametric Mapping, Wellcome Trust Centre for Neuroimaging, Londen, Londen, UK; www.fil.ion.ucl.ac.uk/spm/software/spm8/). Next, segmentation was applied to the MRI resulting in a grey matter (GM) map and a warping into the Montreal Neurological Institute (MNI) space. Then, PET frames were warped into the MNI space using the transformation parameters obtained in the previous steps. This ensued a normalization of the data.

A last step involved smoothing with a 3D isotropic Gaussian kernel of 6 mm full width at half maximum. The automatic anatomic labeling (AAL) atlas[(93)] was used to define the 116 volumes of interest (VOIs) in a user-independent way. A final VOI consisted of the intersection of the subject's GM map (threshold >0,025) with the AAL VOI. To reduce spillover from high activity to low activity regions, we additionally applied a mask which excluded high-uptake values across all subjects for regions with low to moderate uptake. The final VOIs were subsequently used to generate regional time-activity curves (TACs) from the co-registered PET frames.

3.1.4 Kinetic analysis of the PMP PET data

3.1.4.1 Fitting of the parent tracer fraction

To obtain the individual plasma TAC of PMP, for each subject 19 arterial samples were collected starting 10 s after tracer injection up to 80 min. Blood sampling was performed in distinct intervals with the following protocol: every 10 s for the first min, at 1 min each 30 s, at 2 - 5 min every 60 s and every 10 min between 10-80 min. For the assessment of the MBC, 7 additional arterial samples were drawn at 1, 2, 5, 10, 20, 60 and 80 min. Following centrifugation, plasma was collected and the radioactivity was measured in a gamma counter. The samples for MBC were supplementary placed in a HPLC to measure the fraction radioactivity in the plasma representing the parent tracer concentration. To fit the measurements of the parent fraction and thereby interpolating the parent fraction over time, multiple fitting functions were assessed (94) :

1) The mono-exponential function: $\mathrm{F(t)} = \mathrm{Ae}^{\frac{-\ln(2).t}{\alpha}}$

2) The constrained mono-exponential function: $\mathrm{F(t)} = \mathrm{e}^{\frac{-\ln(2).t}{\alpha}}$

with F(t) and A describing the intact tracer over time and the amplitude respectively, while α defines the biological half life of the radionuclide, which was in this study ^{11}C.

3) The bi-exponential function: $\mathrm{F(t)} = \mathrm{Ae}^{\frac{-\ln(2)t}{\alpha}} + \mathrm{Be}^{\frac{-\ln(2)t}{\beta}}$

4) The constrained bi-exponential function: $\mathrm{(t)} = \mathrm{Ae}^{\frac{-\ln(2).(t-t_{delay})}{\alpha}}$ + (1-A) $\mathrm{e}^{\frac{-\ln(2).(t-t_{delay})}{\beta}}$

in which A and B are the amplitudes of the two processes each described by a half-life of α and β respectively. For the constrained function a time-constant delay was included, which represents the delay before metabolisation takes place.

5) The Hill function: $\mathrm{F(t)} = \frac{1}{1+(\frac{a}{t})^n}$

where a and n are parameters that describe respectively the time to obtain half of the maximum value and the steepness of the slope.

MBC was performed on each individual plasma TAC before further model analysis. For this correction a type of fitting function was used to express the fraction authentic tracer remaining at time t as the product of the plasma curve and the fitted authentic fraction.

3.1.4.2 Compartmental models

The 2T3k model for PMP developed by Koeppe et al.[4] was used. In addition, to check for the irreversible nature of PMP, another compartmental model i.e. a two-tissue four-rate constant (2T4k) model was tested. Both were implemented in-house using Matlab (MATLAB and StatisticsToolbox Release 2013a, The MathWorks, Inc., Natick, Massachusetts, United States).

The 2T3k model for the PMP tracer consists of one arterial blood compartment and two tissue compartments within the brain (figure 3.1). The first tissue compartment indicates the tissue concentration of the authentic tracer C_{free}, whereas the second compartment in the tissue refers to the concentration of hydrolyzed metabolite C_m. PMP is a tracer analogue of Ach that is lipophilic enough to cross the blood brain barrier. Once transported from the blood into the brain tissue, tracer molecules can partly be transported back to the blood or can get trapped. PMP trapping occurs when the tracer is metabolized into its hydrophilic state by the specific action of the enzyme AchE. The entire process is described by three rate constants: K_1 defines influx from the blood to the brain, k_2 describes the transport back into the blood and k_3 is the hydrolysis rate of the enzyme AchE, the clinical parameter of interest.

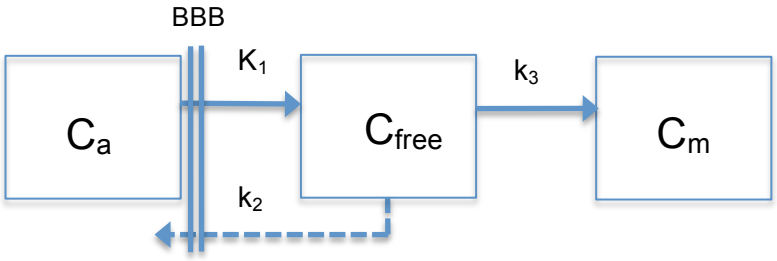

Figure 3.1 Schematic representation of the irreversible compartmental model of the PMP tracer. This two – tissue three-rate model is defined by two tissue compartments, an arterial blood pool C_a and three rate constants (K_1, k_2 and k_3). Influx from the blood to the brain is defined by K_1, whereas k_2 refers to the efflux from the brain tissue back into the blood pool. Tracer transport from the tissue concentration of the authentic tracer (C_{free}) to the metabolized concentration (C_m) is determined by the rate constant k_3. BBB= blood brain barrier

The changes in tissue concentration of the tracer over time within the free and metabolized compartment are represented by differential equations. The following pair of equations describes the kinetics of the PMP tracer in tissue:

$$\frac{dC_{free}(t)}{dt} = K_1 C_a(t) - (k_2 + k_3) C_{free}(t)$$

$$\frac{dC_m(t)}{dt} = k_3 C_{free}(t)$$

with C_{free} and C_m respectively the concentration of the authentic and metabolized tracer concentration in cerebral tissue. C_a represents the authentic tracer concentration in the blood

compartment but since in our study whole blood was not analyzed, plasma samples corrected for brain metabolites were used instead.

The total radioactivity in the brain tissue C_T is composed of the two types of tissue concentration i.e. authentic and metabolized tracer concentration:

$$C_T = C_m + C_{free}$$

The following solution can be derived for the 2T3k model:

$$C_T(t) = \frac{K_1 k_2}{k_2 + k_3} \int_0^t C_a(\tau)\, e^{-(k_2+k_3)(t-\tau)} d\tau + \frac{K_1 k_3}{k_2 + k_3} \int_0^t C_a(\tau) d\tau \qquad [1]$$

The three model parameters were estimated by fitting the regional tissue TAC to this theoretical function (derived from the compartmental model and the input function) using non-linear least squares (NLS) optimization.

The total radioactive PET signal within a cerebral VOI is composed of the signals from both the tissue and the vascular pool in the brain. To investigate the contribution of the brain vascular pool, parameter V_b i.e. the fraction of tissue volume occupied by vascular blood, was either added or excluded. In total three subtypes of the 2T3k model were investigated:

1. Without V_b: 2T3k
2. With V_b as an additional parameter and using the plasma input function corrected for metabolites in the plasma as a measure for the vascular pool in the brain (V_b^{cor}): 2T3k+V_b^{cor}.
3. With V_b as an additional parameter and using the plasma input function not corrected for metabolites in the plasma as a measure for the vascular pool in the brain (V_b^{uncor}): 2T3k+V_b^{uncor}.

The tracer concentration in the vascular pool can be calculated using the arterial whole blood concentration but since these data were not available in our study, the plasma concentration either corrected or uncorrected for metabolites was used as a surrogate. For the subtypes 2 and 3, the theoretical equation [1] is extended and represented by:

$$C_{tot}(t) = C_T(t) + V_b C_p(t)$$

where C_{tot} is the total radioactive concentration measured by PET. For this study specifically, V_b defines the plasma fraction of tissue volume occupied by vascular blood and C_p is the plasma concentration, either corrected or uncorrected for metabolites in the brain. The parameters of each subtype model were estimated by fitting the regional tissue TAC to the theoretical function with NLS optimization, using the metabolite-corrected plasma TAC as the input function.

In case of the 2T4k reversible model of PMP, an extra rate constant k_4 was added (figure 3.2). This rate constant describes the tracer transport from the metabolite tissue compartment to the authentic tracer tissue compartment in case the tracer metabolite is de-metabolized and/or efflux of metabolites out of the metabolite compartment is assumed likely. The tracer behavior in the 2T4k model is described by the following set of differential equations (94):

$$\frac{dC_{free}(t)}{dt} = K_1 C_a(t) - (k_2+k_3)C_{free}(t) + k_4 C_m(t)$$

$$\frac{dC_m(t)}{dt} = k_3 C_{free}(t) - k_4 C_m(t)$$

where C_{free} and C_m denotes the free tracer and metabolized concentration respectively. C_T is obtained by rewriting these equations:

$$C_T(t) = C_{free}(t) + C_m(t) = \left(\varphi_1 e^{-\theta_1 t} + \varphi_2 e^{-\theta_2 t}\right) \otimes C_a(t)$$

with:

$$\varphi_1 = \frac{K_1(\theta_1 - k_3 - k_4)}{\Delta} \; and \; \varphi_2 = \frac{K_1(\theta_2 - k_3 - k_4)}{-\Delta}$$

$$\theta_1 = \frac{k_2 + k_3 + k_4 + \Delta}{2} \; and \; \theta_2 = \frac{k_2 + k_3 + k_4 - \Delta}{2}$$

$$\Delta = \sqrt{(k_2 + k_3 + k_4)^2 - 4k_2k_4}$$

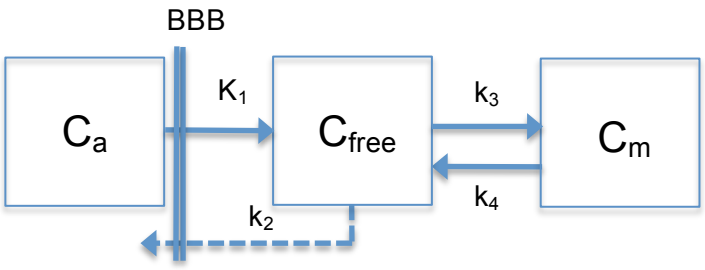

Figure 3.2 Schematic representation of the reversible compartment model of the PMP tracer. This two–tissue four-rate constant model is defined by two tissue compartments, an arterial blood pool Ca and four rate constants (K_1, k_2, k_3 and k_4). Influx from the blood to the brain tissue is defined by K_1, whereas k_2 refers to the efflux from the brain back into the blood. Tracer transport from the tissue concentration of the authentic tracer (C_{free}) to the metabolized concentration (C_m) is determined by the rate constant k_3. Transport of the (de)-metabolized tracer back into the authentic tracer compartment is defined by the rate constant k_4.

The same three subtype models as applied with the 2T3k model were also investigated using the 2T4k model: 2T4k (V_b=0), 2T4k+V_b^{cor} and 2T4k+V_b^{uncor}. The model parameters were estimated by fitting the regional tissue TAC to the theoretical function with NLS optimization, using the metabolite-corrected plasma TAC as input.

3.1.4.3 Reference method

The reference method (REF) by Zundorf et al.[91] was used in this study, with the putamen as reference region. The general concept of the REF for the PMP tracer is based upon the assumption that the reference region has a very high hydrolysis rate such that k_3 >> k_2. This feature assumes the PMP kinetics within the reference region to be described by the one-tissue one-rate constant model (1T1k), as pictured in figure 3.3.

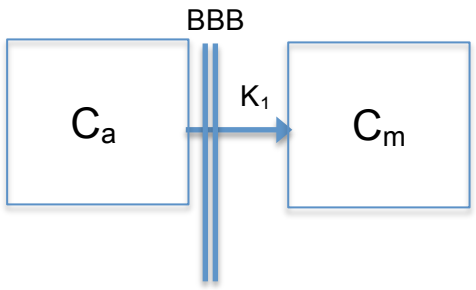

Figure 3.3 Schematic representation of the PMP reference method. K_1 is the rate constant that defines the influx across the blood brain barrier (BBB) from the arterial blood compartment (C_a) towards the brain compartment with metabolized tracer concentration (C_m).

Almost every PMP tracer molecule that enters the reference region is assumed being trapped such that efflux can be ignored. The mathematical equation for the 1T1k model in a region with high AchE hydrolysis is the following:

$$C_R(t) = K_1^R \int_0^t C_a(\tau)\, d\tau \qquad [2]$$

with C_R the tracer concentration in the reference region and K_1^R the rate constant defining PMP influx into the brain reference tissue. C_a refers to the input function, which is defined by the concentration of authentic PMP tracer present in blood.

Combining this model of the reference region with the solution of the 2T3k model (equations [1] and [2]) allows removal of the input function. Herholz et al.[90] proposed the target-tissue activity to reference-tissue activity ratio to get an estimate of k_3 without input function:

$$C(t) = \frac{C_T(t)}{C_R(t)} = A\, w(t) + B \qquad [3]$$

with $$w(t) = \frac{\int_0^t C_a\ (\tau)e^{-K(t-\tau)}d\tau}{\int_0^t C_a(\tau)d\tau} \qquad [4]$$

and:

$A=\frac{K_1}{K_1^R} \cdot \frac{k_2}{k_2+k_3}$

$B=\frac{K_1}{K_1^R} \cdot \frac{k_3}{k_2+k_3}$

$K= k_2 + k_3$

To estimate the parameters A, B and K using the NLS fit, one assumes that the function w(t) can be approximated by a mono-exponential decline resulting in:

$$C(t) = Ae^{-Kt} + B$$

The rate constant k_3 can then be calculated from A, B and K by: $k_3 = \frac{B}{A+B}K$.

To remove the assumption of a mono-exponential decline of function w(t), Zundorf et al.[91] developed a technique to calculate w(t) by means of partial and numerical integration. The use of equation [2] together with partial integration of equation [3] gives a novel w(t):

$$w(t) = 1 - K\frac{\int_0^t C_R(\tau)e^{K(t-\tau)}d\tau}{C_R\ (\tau)} \qquad [5]$$

When [5] filled in at equation [3] gives rise to the following equation:

$$C(t) = A\left[1 - K\frac{\int_0^t C_R(\tau)e^{K(t-\tau)}d\tau}{C_R\ (\tau)}\right] + B$$

Now the three model parameters A, B and K are estimated using the NLS fit technique without the unnecessary assumption made by Herholz et al. (90).

3.1.4.4 Shape analysis

The shape analysis (SA) estimates the k_3 values solely from the shape of the regional brain TAC, based on the following four assumptions (4):

$C_{free}\ (t_0) = C_{tot}\ (t_0)$ and $C_m\ (t_0) = 0$

$C_{free}\ (t_{final}) = 0$ and $C_m\ (t_{final}) = C_{tot}\ (t_{final})$

$C_{free}\ (t_n) = C_{tot}\ (t_n) - C_m\ (t_n)$ i.e. we assume $V_b = 0$

$C_m\ (t_n)= k_3\ C_{free}\ (t_n\text{-}1)\ \Delta t + C_m\ (t_n\text{-}1)$

with t_0 and t_{final} respectively the start and the end time of the scan session. Note that start of injection parallels with the start of scanning. To improve numerical accuracy, PET data were interpolated such that the time interval Δt is much shorter than the scan frame time. This gave rise to novel time frames as defined by t_n, with n defining the frame number.

The assumptions define clearly that at the start of the scan time no metabolites might be formed yet in the brain such that the total concentration in the brain equals the authentic tracer concentration. On the contrary at the end of the scan period only metabolites and no authentic tracer molecules should be left. Therefore, at the final PET frame the radioactive concentration in the metabolite compartment should only contribute to the tissue tracer signal. The parameter k_3 needs to be estimated such that $[C_m\ (t_{final}) - C_{tot}\ (t_{final})]^2$ is minimal.

3.1.5 Statistics

Each statistical analysis was performed at the VOI level, implicating that all 116 VOIs from the AAL atlas were analyzed individually, thereby correcting for multiple comparisons using the method of false discovery rate (FDR), except if mentioned otherwise. The 116 VOIs of the AAL atlas were grouped logically over 10 brain regions. Each region contains a set of VOIs from the AAL atlas (table S-II supplementary material). To generate a compact overview of the study results, per brain region the mean of the VOIs was calculated. Thus, not the result per individual VOI were displayed but the mean result for a set of VOIs from the AAL atlas associated with one of the 10 brain regions. All statistics were carried out with in-house scripts and Matlab (MATLAB and StatisticsToolbox Release 2013a, The MathWorks, Inc., Natick, Massachusetts, United States). Outliers were detected and removed from each analysis. An outlier was defined as follows: either when estimated model parameters were equal to one of the boundaries values, either when the values were below Q1-1.5*IQR or above Q3+1.5*IQR with Q1 and Q3 denote respectively the upper and lower quartile and IQR the interquartile range. Mean values, SD and coefficient of variation (COV) of the model parameters were calculated for all model analyses and every group of subjects (PPA, HC and MCI).

To find the best model among a set of candidates, Akaiki criteria[95] (AIC) and Schwarz criteria[96] (SC) were used. Both are methods for assessing a model fit including penalties for the number of estimated parameters. AIC and SC are given by the following formula:

$$\mathrm{AIC} = \mathrm{N} \ln\left(\frac{SS}{N}\right) + 2P$$

$$\mathrm{SC} = \mathrm{N} \ln\left(\frac{SS}{N}\right) + \mathrm{P} \ln\left(\mathrm{N}\right)$$

with N= number of frames, SS= sum of square differences between the measurement and the model predication and P= number of parameters.

For the MBC analysis, using AIC and SC, five fitting functions (see 3.1.4.1) were compared to find the function that overall fits best the authentic tracer fraction. This was done for a total of 47 cases, which indicate the number of subjects with a first scan plus the number of subjects with a second scan. The effect of excluding later samples on the choice of the fitting function for MBC was examined using a paired t-test with a significance level of 0.05. Here the values of k_3 derived from two analyses, one including all plasma samples and one with only the samples until 40 min, were compared with for both analyses the Hill function as fitting function for MBC.

The irreversible character of PMP and the improvement of model fitting by addition of the model parameter V_b were studied by comparing the AIC and SC from six different models. For each main model that was either the 2T3k or 2T4k model, three subtypes were studied (see 3.1.4.2). This analysis was performed using all scans (n=47). The best compartmental model to describe the PMP kinetics was chosen for each VOI separately, followed by the study of the general best model per brain region and this for all scans and per subject group.

For the comparison analysis of the best invasive method and the two non-invasive models REF and SA, both a Pearson correlation and Bland-Altman analysis were used. Now the best invasive model was considered as the standard model on which the reliability of the non-invasive k_3 estimates was tested. ANOVA and paired t-tests with a significance level of 0.05 were performed to assess across the three methods (REF, SA and best invasive model) the significant differences in the following three components i.e. variability in k_3 values, k_3 and test-retest values. No FDR for multiple comparisons was applied. For all these analyses only the HC scans, both baseline and follow-up (n=14), were used. In addition, boxplots were produced to represent the dispersion of the data.

To compare the HC and the patient groups at baseline with regard to regional k_3 values, exploratory unpaired t-tests with a significance level of 0.05 were applied. In addition to the investigation at baseline, also differences between scan 1 and 2 were examined. Both relative [(k_3 scan2- k_3 scan1/ k_3 scan1] and absolute (k_3 scan2- k_3 scan1) differences in k_3 between the control group and patient groups were studied (HC vs. MCI and HC vs. PPA) using unpaired t-tests with a significance level of 0.05. For this statistical analysis only the HC and patients (MCI and PPA) of which two scans existed (n=18) were compared among all VOIs. Next to between-group comparisons, also within-group k_3 changes were examined. For the HC this implies a test-retest analysis, whereas for the patient groups this is equivalent to the study of change in k_3 values after galantamine drug treatment. Here, the k_3 values between scan 1 and scan 2 of each subject group were compared using a paired t-test with a significance level of 0.05.

3.2 Results

3.2.1 Search of the best fitting function for the parent fraction

The analysis to find the function that corrects best for metabolites in the plasma designated the Hill function as the best fit in most cases (37 out of the 47 cases). For all cases, the AIC and SC obtained the same functions with best fits. In a second-level analysis, where the samples after 40 min post-injection were excluded, a distinct result was observed. Table 3.1 gives an overview of the five fitting functions with the number of cases for which they obtained the best fit. This is displayed per subgroup of cases and for both the first- and second-level analysis. In the latter, both the bi-exponential delay and the Hill function obtained the best MBC in 18 of the 47 cases. In both the analyses the two types of mono-exponential functions had no good fits, except in one PPA case for the second-level analysis.

Table 3.1 Overview of the best fitting function across all the 47 cases

Fitting function	All samples				Part of the samples (<40 min pi)			
	N° cases				N° cases			
	MCI (n=12)	HC (n=14)	PPA (n=21)	**TOTAL (n=47)**	MCI (n=12)	HC (n=14)	PPA (n=21)	**TOTAL (n=47)**
Mono-exponential con	0	0	0	**0**	0	0	1	**1**
Mono-exponential del	0	0	0	**0**	0	0	0	**0**
Bi-exponential con	1	3	2	**6**	5	3	2	**10**
Bi-exponential del	1	1	2	**4**	5	3	10	**18**
Hill function	10	10	17	**37**	2	8	8	**18**

Data were analyzed using Akaiki and Schwarz criteria. Cases refer to the number of subjects with a first scan plus the number of subjects with a second scan. Abbreviations: MCI= mild cognitive impairment; HC= healthy controls; PPA= primary progressive aphasia and pi= post-injection.

Representative results from the first-level fit (all samples) with five different functions in a HC at baseline are displayed in figure 3.4. For this control case, the Hill function obtained the best fit with the lowest error (0.005) between measured data and fitted data over time, as shown in figure 3.4. The largest errors were present in the fits with the mono-exponential functions (constrained and delay) and the bi-exponential delay function, which is consistent with the results from the comparison analysis. For the second-level analysis similar results were attained (see supplementary material figure S-I).

Comparison of the k_3 values from the first- and the second-level analysis (paired t-test, p_{FDR}=0.0498) showed statistically significant different k_3 estimations for all VOIs, except for one VOI at the cerebellum across all scans (data not shown). Using the AIC and SC it was clear that the first-level analysis obtained consistently for all VOIs the best fits.

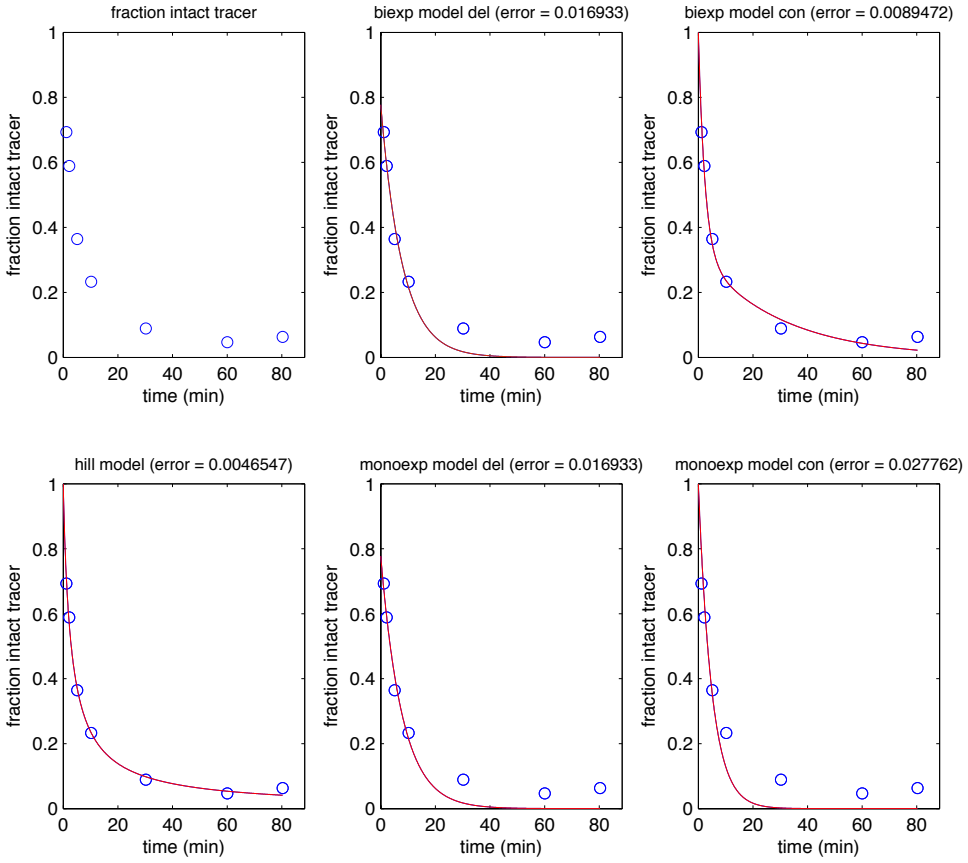

Figure 3.4 Fits for the authentic PMP fraction over time using five distinct functions. The analysis was performed in a healthy control. The error indicates the inaccuracy between the measured and fitted data. Abbreviations: biexp = bi-exponential; monoexp= mono-exponential; del= delay and con= constrained.

3.2.2 VOI-based analysis of the PMP tracer

3.2.2.1 Best model for the PMP analysis in all scans

All scans (both baseline and follow-up, n=47) were included in this analysis and for the MBC the Hill function was applied using all samples. The comparison analysis between the main models 2T3k and 2T4k, comprising each three subtypes (V_b=0, V_b^{cor} and V_b^{uncor}), showed a high preference for the irreversible 2T3k model including V_b as an additional parameter and using the plasma input function corrected for plasma metabolites as a measure for the vascular pool in the brain i.e. the 2T3k+V_b^{cor} model. Of the 116 VOIs, 91 had the 2T3k+V_b^{cor} model as the best analysis for most scans based on AIC and SC.

The choice of the best model across the total of 47 scans and per brain region is displayed in table 3.2. Each brain region is associated with a set of specific AAL VOIs (see supplementary material table S2). Note that for every VOI separately the overall best model was chosen among all the scans. To indicate which subtype model best described per region the scans individually, the percentage of scans for which a certain subtype obtained the best fits is displayed per region of interest (table 3.2). The percentages are mean percentages

because they indicate the mean of the total number of VOIs associated per region with that model as best model to describe the PMP kinetics.

Table 3.2 Best compartmental model for PMP kinetic analysis per region across all scans and all VOIs.

Region	Best main model = 2T3k						Best main model = 2T4k					
	2T3k		2T3k + V_b^{cor}		2T3k +V_b^{uncor}		2T4k		2T4k +V_b^{cor}		2T4k +V_b^{uncor}	
	Best		Best		Best		Best		Best		Best	
Frontal cortex		3,7%	30/30	**76,2%**		9,3%		0%		9,1%		1,7%
Temporal cortex		5,4%	12/12	**77,5%**		8,1%		0%		7,9%		1,0%
Parietal cortex		4,2%	12/12	**76,2%**		9,8%		0%		8,0%		1,8%
Occipital cortex		5,6%	14/14	**73,4%**		9,3%		0%		9,6%		2,0%
Insula		4,7%	02/02	**88,4%**		4,7%		0%		2,3%		0%
Cingulum		4,7%	06/06	**76,7%**		10,5%		0%		6,6%		1,6%
Hippocampus+		4,7%	06/06	**68,0%**		11,1%		0%		13,4%		2,9%
Basal ganglia		6,2%	04/06	**39,1%**		9,3%		0,8%	02/6	34,1%		10,5%
Thalamus		4,7%		29,1%		9,3%		0%	02/2	**44,2%**		12,8%
Cerebellum		6,8%	05/26	13,1%		5,2%		3%	21/26	**57,7%**		14,3%

Data were analyzed using the Akaiki and Schwarz criteria. “Best” refers to the best model in general for a number of the VOIs within that brain region across all scans, with “/” indicating none of the VOIs for that specific region. Percentages indicate the mean percentage of VOIs across all individual scans that preferred a model type per region of interest. +Hippocampus and amygdala. Abbreviations: 2T3k model= two-tissue three-rate constant model; 2T4k model= two-tissue four-rate constant model; V_b^{cor}= plasma fraction with a plasma input corrected for metabolites; V_b^{uncor}= plasma fraction with a plasma input uncorrected for metabolites.

For the remaining 25 VOIs the reversible variant i.e. the 2T4k+V_b^{cor} model obtained the lowest AIC and SC. Those VOIs belonged to the high hydrolysis regions such as the cerebellum, basal ganglia and thalamus. On the contrary for all cortical regions the irreversible 2T3k+V_b^{cor} model described best the data.

On the subgroup level, the comparison analysis of the 2T3k+V_b^{cor} and 2T4k+V_b^{cor} model still obtained preference for the 2T3k+V_b^{cor} model at the cortical regions. The percentages of scans for which a subtype model described best the data could differ regionally per group (data not shown). Overall the HC and MCI group had higher regional percentages for the 2T3k+V_b^{cor} model than the PPA group.

Typical results of fitting the brain TAC of a VOI from the frontal cortex (frontal inferior operculum, right hemisphere) using the 2T3k+V_b^{cor} and 2T4k+V_b^{cor} model in a HC are displayed in figure 3.5. For both the AIC and SC criteria, the values were lower for the 2T3k+V_b^{cor} model (figure 3.5). On the contrary the fit with the TAC of the cerebellum VOI (cerebellum 6, right hemisphere) in the same HC obtained the lowest AIC and SC values for the 2T4k+V_b^{cor} model, as pictured in figure 3.6. In this cerebellum VOI, the bias in the fit with the 2T3k+V_b^{cor} model was visually improved using the 2T4k+V_b^{cor} model (figure 3.6).

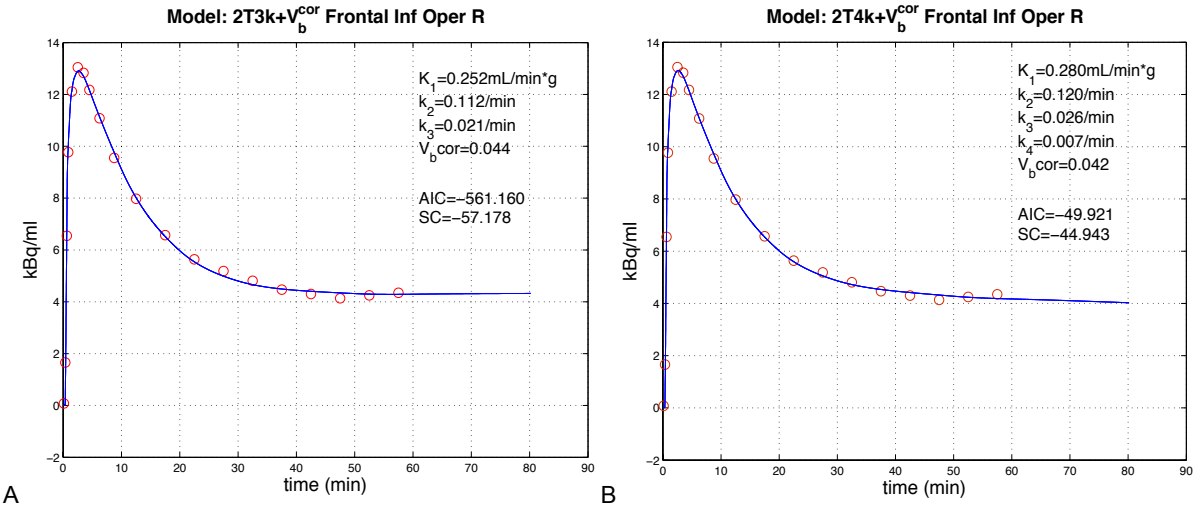

Figure 3.5 Curve-fitting of the right frontal inferior operculum time-activity curve in a healthy control. A. Curve-fitting by the 2T3k+V_b^{cor} model. B. Curve-fitting by the 2T4k+V_b^{cor} model. Abbreviations: 2T3k+V_b^{cor} model= two-tissue three-rate constant model including a plasma fraction with an input corrected for metabolites; 2T4k+V_b^{cor} model= two-tissue four-rate constant model including a plasma fraction with an input corrected for metabolites; R= right; AIC= Akaiki criteria and SC= Schwarz criteria.

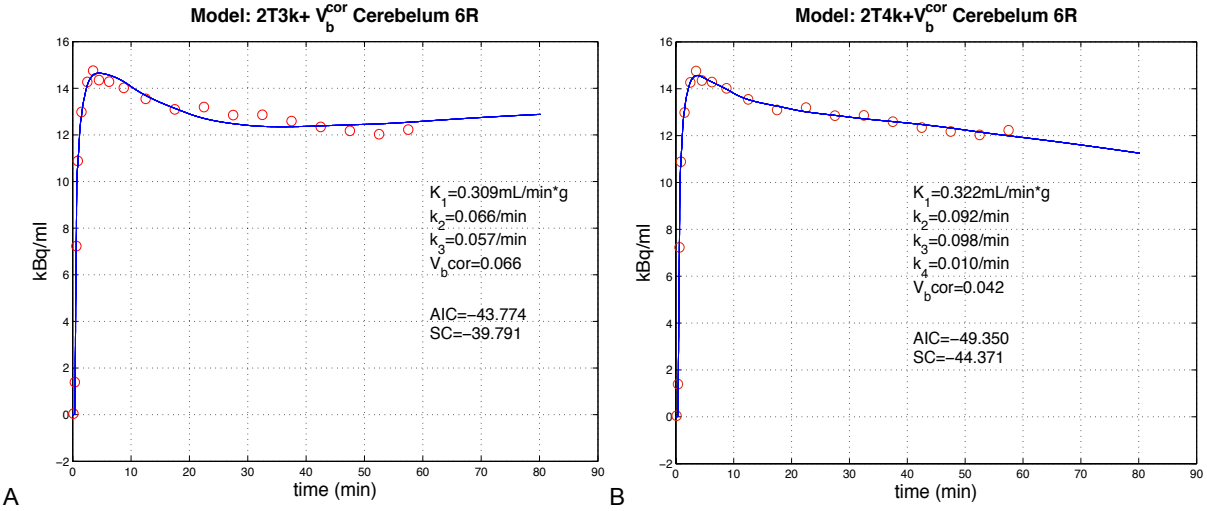

Figure 3.6 Curve-fitting of the right cerebellum 6 time-activity curve in a healthy control. A. Curve-fitting by the 2T3k+V_b^{cor} model B. Curve-fitting by the 2T4k+V_b^{cor} model. Abbreviations: 2T3k+V_b^{cor} model= two-tissue three-rate constant model including a plasma fraction with a plasma input corrected for metabolites; 2T4k+V_b^{cor} model= two-tissue four-rate constant model including a plasma fraction with a plasma input corrected for metabolites; R= right; AIC= Akaiki criteria and SC= Schwarz criteria;

In the control group, the regional mean of each rate constant, estimated from the 2T3k+V_b^{cor} model, was calculated for all 10 brain regions. The value of the regional mean is the mean of

a model parameter (K_1, k_2 or k_3) from a set of VOIs per brain region. Also the COV and SD were calculated. Table 3.3 shows the mean, SD and COV of each rate constant estimated with the 2T3k+V_b^{cor} model. The data were derived from the baseline scans (n=9) of the HC group. In the neocortical regions, the mean K_1 values had a range from 0.348 to 0.364 mL/min·g with COV ranging from 17.6 to 23.6%, as displayed in table 3.3. The highest mean for K_1 was estimated in the thalamus region, whereas the lowest value was obtained in the hippocampus and amygdala. The mean cortical k_2 values ranged from 0.123 to 0.138 min^{-1} with the COV ranging form 13.2 up to 22.7%. The thalamus had the highest mean k_2 value and the basal ganglia the lowest. For the mean k_3 values of the cortical regions, the COV ranged from 11.2 to 12.9% and the value range was: 0.020 to 0.022 $min^{-1.}$ The highest k_3 values were observed in the cerebellum, followed by the thalamus and the striatum, whereas the lowest mean k_3 values were obtained in the parietal cortex.

Table 3.3 Baseline values of the regional rate constants K_1, k_2 and k_3 in all healthy controls using the 2T3k+V_b^{cor} model.

Brain region	K_1 (mL · min^{-1}· g^{-1})		k_2 (min^{-1})		k_3 (min^{-1})	
	Mean ± SD	COV (%)	**Mean** ± SD	COV (%)	**Mean** ± SD	COV (%)
Frontal cortex	***0.348*** ± *0.068*	*19.6*	***0.130*** ± *0.021*	*16.3*	***0.022*** ± *0.003*	*11.7*
Temporal cortex	***0.357*** ± *0.084*	*23.6*	***0.123*** ± *0.028*	*22.7*	***0.021*** ± *0.003*	*12.9*
Parietal cortex	***0.355*** ± *0.067*	*19.0*	***0.131*** ± *0.017*	*13.2*	***0.020*** ± *0.002*	*11.2*
Occipital cortex	***0.365*** ± *0.064*	*17.6*	***0.138*** ± *0.024*	*17.5*	***0.021*** ± *0.003*	*12.0*
Hippocampus+	***0.289*** ± *0.055*	*19.0*	***0.095*** ± *0.016*	*16.5*	***0.027*** ± *0.004*	*13.6*
Cingulum	***0.403*** ± *0.077*	*19.0*	***0.137*** ± *0.025*	*18.0*	***0.023*** ± *0.002*	*10.2*
Insula	***0.376*** ± *0.071*	*18.9*	***0.122*** ± *0.018*	*14.7*	***0.023*** ± *0.003*	*11.0*
Basal ganglia	***0.343 ±*** *0.067*	*19.6*	***0.029*** ± *0.014*	*47.4*	***0.042*** ± *0.013*	*29.8*
Thalamus	***0.457 ±*** *0.083*	*18.1*	***0.151*** ± *0.018*	*12.0*	***0.047*** ± *0.005*	*9.8*
Cerebellum	***0.341 ±*** *0.068*	*19.8*	***0.079*** ± *0.021*	*26.0*	***0.067 ±*** *0.015*	*22.6*

Analysis was performed on a VOI-based level using the 2T3k+V_b^{cor} model in healthy controls. +Hippocampus and amygdala. Abbreviations: 2T3k+V_b^{cor} model= two-tissue three-rate constant model including a plasma fraction with a plasma input corrected for metabolites; SD= standard deviation; COV= coefficient of variation and VOI= volume of interest.

Figure 3.7A illustrates the heterogeneous distribution of PMP in the brain during the total scan time period of 60 min and this for the same cerebral slice from a HC. For each scan frame of the dynamic PET sequence i.e. 4x15 s, 4x1 min, 2x2.5 min and 10x5 min, the PMP distribution is displayed for the same slice in a HC brain. For the last 30 min of scanning, a

sum image from the total group of HC was made, as displayed in figure 3.7B. Here slices through the whole brain are shown to illustrate the regional tracer radioactivity in the brain of HC.

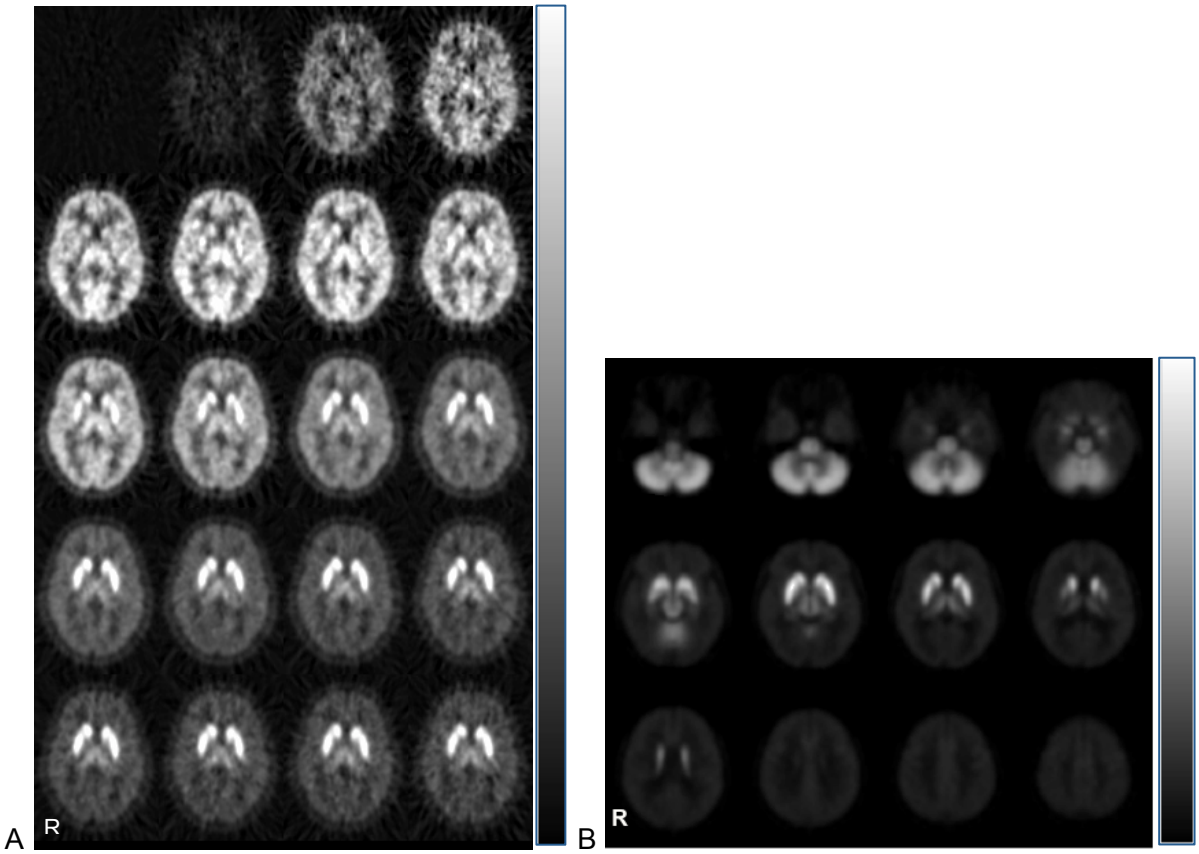

Figure 3.7 PET scan slices representing the regional PMP distribution in the brain. A. Distribution of the PMP tracer over the total scan time of 60 min (4x15 s, 4x1 min, 2x2.5 min and 10x5 min) in the same brain slice of a healthy control. B. Distribution of the PMP tracer in cerebral slices when summing the last 30 min of all nine healthy controls. The grey scale on the right sight indicate high (white) and low (black) PMP uptake. Images are in radiological orientation (right). Abbreviation: R= right.

3.2.2.2 Comparison 2T3k+V_b^{cor} and the non-invasive models

For the comparison between the invasive model and two non-invasive models, the overall best invasive compartmental model (2T3k+V_b^{cor} model) obtained in the previous analysis was now used to evaluate the usability of the SA and REF to estimate k_3. This analysis was limited to the group of HC of which only cortical VOIs were assessed. In total nine subjects of whom five had a repeat scan were analysed.

Table 3.4 gives the regional k_3 values estimated by the three methods, including the COV values. By using SA, k_3 estimates showed a COV ranging from 12.4 to 33.2%. For the standard and the REF model this was respectively 9.8 to 29.8% and 12.0 to 47.4%. The thalamus obtained the lowest and the basal ganglia the highest COV for both the REF and the 2T3k+V_b^{cor} model, whereas for the SA the parietal cortex and the cerebellum obtained respectively the lowest and highest COV.

Table 3.4 Mean regional k_3 values per model in healthy controls at baseline.

Brain region	2T3k+V_b^{cor} k_3 (min^{-1})		REF k_3 (min^{-1})		SA k_3 (min^{-1})	
	Mean ± SD	COV (%)	Mean ± SD	COV (%)	Mean ± SD	COV (%)
Frontal cortex	*0.022 ± 0.002*	*10.7*	0.052 ± *0.085*	*16.3*	*0.028±0.005*	*17.6*
Temporal cortex	*0.021 ± 0.003*	*12.9*	*0.035 ± 0.039*	*22.7*	*0.027±0.004*	*16.5*
Parietal cortex	*0.020 ± 0.002*	*11.2*	*0.027 ± 0.023*	*13.2*	*0.025±0.003*	*12.4*
Occipital cortex	*0.021 ± 0.003*	*12.0*	*0.019 ± 0.014*	*17.5*	*0.026±0.005*	*17.0*
Hippocampus+	*0.027 ± 0.004*	*13.6*	*0.137 ± 0.153*	*16.5*	*0.037±0.010*	*26.4*
Cingulum	*0.023 ± 0.002*	*10.2*	*0.058 ± 0.051*	*18.0*	*0.028±0.004*	*15.3*
Insula	*0.023 ± 0.003*	*11.0*	*0.072 ± 0.054*	*14.7*	*0.029±0.004*	*14.5*
Basal ganglia	*0.042 ± 0.013*	*29.8*	*0.059 ± 0.173*	*47.4*	*0.082±0.025*	*30.2*
Thalamus	*0.047 ± 0.005*	*9.8*	*0.053 ± 0.038*	*12.0*	*0.059±0.018*	*30.8*
Cerebellum	*0.067 ± 0.015*	*22.6*	*0.107 ± 0.196*	*26.0*	*0.070±0.023*	*33.2*

Only the baseline scans from the healthy control group were used, of which all 116 VOIs were analyzed individually. For each of the 10 brain regions, mean k_3 values were calculated using the k_3 values of the VOIs comprised per region. Abbreviations: 2T3k+V_b^{cor}= two-tissue three-rate constant model including a plasma fraction with a plasma input function corrected for metabolites; REF= reference method; SA= shape analysis, SD= standard deviation and COV= coefficient of variation.

With the putamen as the reference region, the k_3 estimates from the REF and the 2T3k+V_b^{cor} model weakly correlated significantly (r=0.28; paired t-test, $p<10^{-9}$). This linear positive correlation between the REF and 2T3k+V_b^{cor} model is displayed in figure 3.8A. The differences in k_3 estimations between both methods have the trend to increase with higher values for k_3. For the association of the k_3 values between the SA and the 2T3k+V_b^{cor} model, a medium significant correlation (r=0.40; paired t-test, $p<10^{-20}$) was obtained. For the SA, the linear positive correlation with the 2T3k+V_b^{cor} model is displayed in figure 3.9A.

Bland-Altman analyses were used to plot the agreement in k_3 values between the invasive best model i.e. the 2T3k+V_b^{cor} model and the non-invasive models REF and SA, as shown in figure 3.8B and 3.9B. The average discrepancy (bias) between the k_3 values of the 2T3k model vs. REF and SA was respectively -0.006 and -0.007 (full line displayed in figure 3.8B and 3.9B). The 5% and 95% percentile of the REF were larger than for the SA model, as indicated by the dotted lines in correspondingly figure 3.8B and 3.9B.

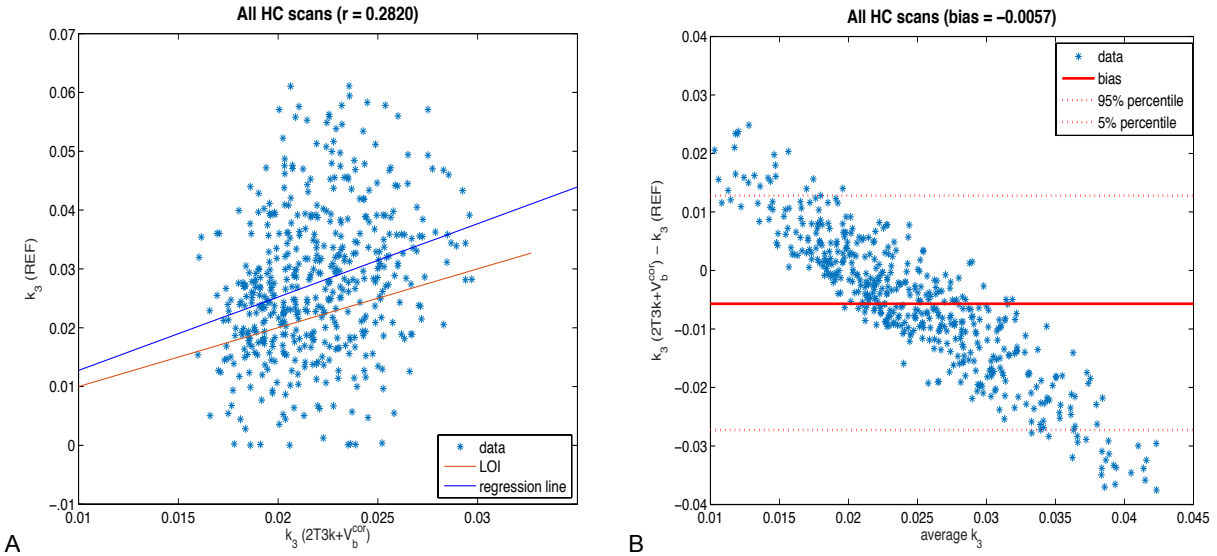

Figure 3.8 Comparison analyses between the REF and 2T3k+V_b^{cor} model using all scans of the HC. Only cortical VOIs were analyzed. A. Pearson correlation analysis. B. Bland-Altman plot. Here upper and lower dotted lines define respectively the 95% (0.0128) and 5% (-0.0273) percentile. Abbreviations: HC= healthy controls; REF= reference method; 2T3k+V_b^{cor} model= two-tissue three-rate constant model including a plasma fraction with a plasma input corrected for metabolites; LOI= line of identity and VOI= volume of interest.

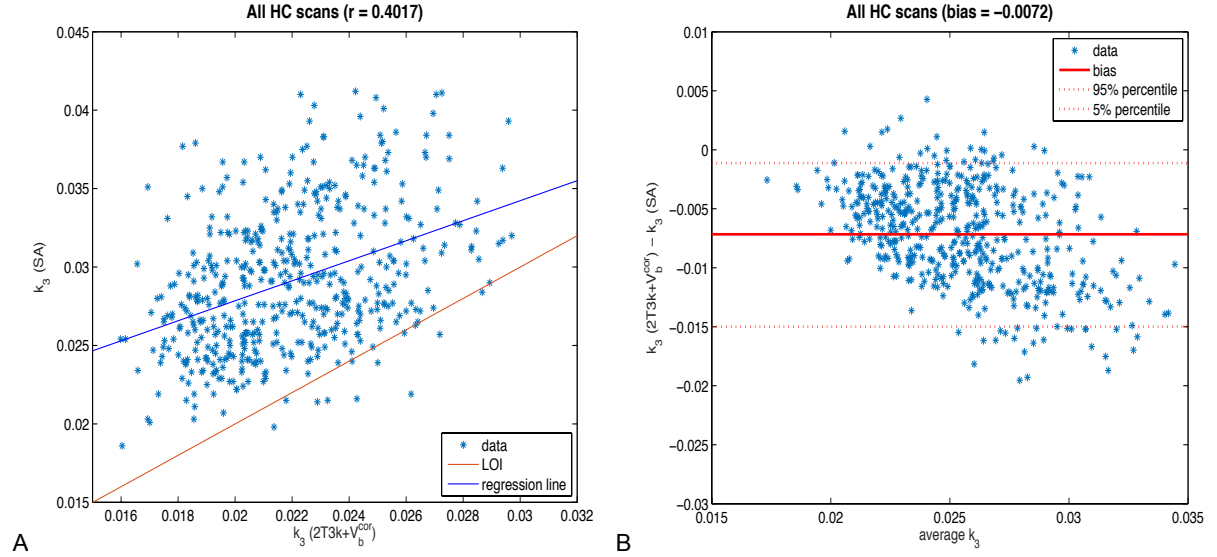

Figure 3.9 Comparison analyses between the SA and 2T3k+V_b^{cor} model using all scans of the HC. Only cortical VOIs were analyzed. A. Pearson correlation analysis. B. Bland-Altman plot. Here the upper and lower dotted lines define respectively the 95% (-0.0011) and 5% (-0.0150) percentile. Abbreviations: HC= healthy controls; SA= shape analysis; 2T3k+V_b^{cor} model= two-tissue three-rate constant model including a plasma fraction with a plasma input corrected for metabolites; LOI= line of identity and VOI= volume of interest.

The variability of k_3 values for each model (best invasive model, REF and SA) is shown in figure 3.10A. The 2T3k+V_b^{cor} model showed the smallest variability (IQR = [0.0196; 0.0238]/min) and the REF the highest (IQR = [0.0187; 0.0375]/min). The mean k_3 values were significantly different among the three methods (ANOVA, $p<10^{-10}$) and the 2T3k+V_b^{cor} model was significantly different from the REF and SA (paired t-tests, $p < 10^{-9}$ in both cases). The method 2T3k+V_b^{cor} also showed the lowest amplitudes of the test-retest values (IQR = [-5.76; 8.97]%), as displayed in Figure 3.9C. The test-retest values of the three methods were

significantly different (ANOVA, $p<10^{-10}$). If we limited our analysis to the baseline scans only, the variability of the methods was similar as taking all scans together (figure 3.10A and B).

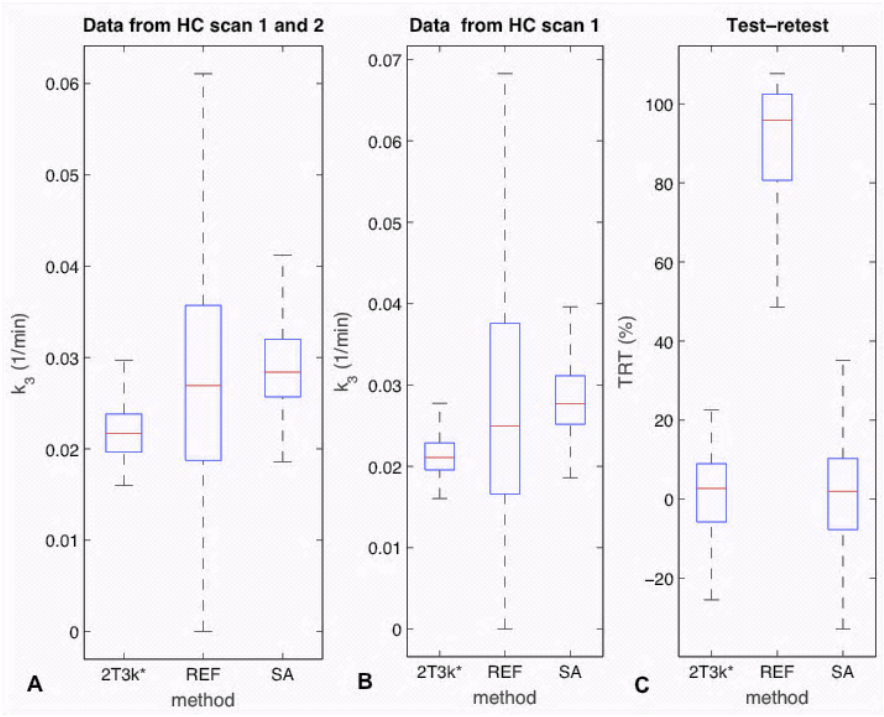

Figure 3.10 Boxplots of the k_3 values of healthy controls using three different models. A. All 47 scans have been used of which only the cortical VOIs were evaluated. B. Only the baseline scans were assessed C. Test-retest. Abbreviations: HC= healthy controls; 2T3k*= 2T3k+V_b^{cor} model (two-tissue three-rate constant model including a plasma fraction with a plasma input corrected for metabolites); REF= reference method; SA= shape analysis and TRT= test-retest.

3.2.2.3 Differences in k_3 values between healthy controls and patient groups

Next to the healthy subjects, for each group of patients i.e. PPA and MCI patients, model parameters were estimated both at baseline (scan 1) and after treatment (scan 2) using the 2T3k+V_b^{cor} model. For the group of HC, k_3 estimations of a repeat scan (scan 2) were performed to obtain test-rest results.

Baseline k_3 values from the MCI patients obtained in almost all regions, except for the frontal cortex, lower values as compared to the PPA patient group and the HC (figure 3.11). All three groups obtained at baseline the highest k_3 values for the cerebral regions cerebellum, thalamus and basal ganglia, whereas the cortical regions consistently had the lowest values for k_3. The PPA patients had consistently lower values for the rate constant k_2 among all brain regions (table S-III in supplementary material). Also the influx in the brain, as represented by K_1, was constantly lower for this patient group. However, the COV values for all model parameters were the highest in the PPA patient group for most of the brain regions. In general, the control group obtained the lowest COV values for all three the rate constants of the 2T3k+V_b^{cor} model (data not shown).

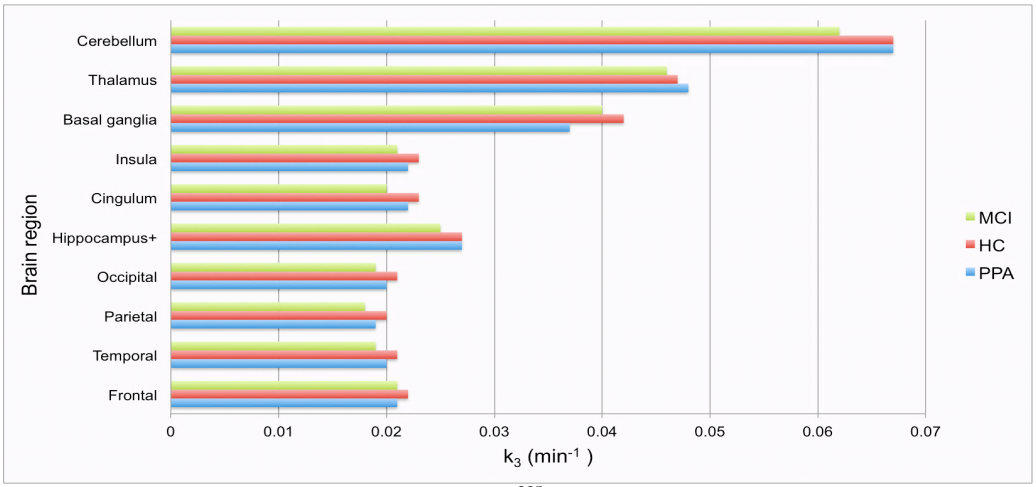

Figure 3.11 Baseline k_3 values using the 2T3k+V_b^{cor} model, displayed per brain region and group of subjects. +Hippocampus and amygdala. Abbreviations: 2T3k+V_b^{cor} model= two-tissue three-rate constant model including the plasma fraction with a plasma input corrected for metabolites; MCI= mild cognitive impairment; HC= healthy controls and PPA= primary progressive aphasia.

Mean values and SDs of the regional k_3 estimates for scan 1 and 2 per group of subjects are displayed in table 3.5. The region with the highest k_3 values among all subgroups and for both scan 2 and 1 is the cerebellum followed by the thalamus and the basal ganglia. An exception is present for the MCI patient group that obtained in scan 2 at the basal ganglia higher k_3 values than at the thalamus. The lowest k_3 values are estimated consistently, for both the three groups and the two scans, at the parietal cortex.

Table 3.5 Regional k_3 values per subgroup of subjects for scan 1 and 2 using the 2T3k+V_b^{cor} model.

Brain region	**PPA mean k_3 (min^{-1})**		**HC mean k_3 (min^{-1})**		**MCI mean k_3 (min^{-1})**	
	Scan 1	Scan 2	Scan 1	Scan 2	Scan 1	Scan 2
Frontal cortex	**0.021**±0.003	**0.018**±0.003	**0.022** ± 0.003	**0.023**±0.003	**0.021**±0.004	**0.018**±0.003
Temporal cortex	**0.020**±0.004	**0.017**±0.004	**0.021** ± 0.003	**0.022**±0.003	**0.019**±0.004	**0.017**±0.004
Parietal cortex	**0.019**±0.003	**0.016**±0.003	**0.020** ± 0.002	**0.021**±0.003	**0.018**±0.003	**0.016**±0.003
Occipital cortex	**0.020**±0.003	**0.017**±0.004	**0.021** ± 0.003	**0.021**±0.003	**0.019**±0.004	**0.016**±0.003
Hippocampus+	**0.027**±0.006	**0.023**±0.006	**0.027** ± 0.004	**0.028**±0.005	**0.025**±0.006	**0.021**±0.004
Cingulum	**0.022**±0.003	**0.018**±0.003	**0.023** ± 0.002	**0.023**±0.002	**0.020**±0.004	**0.018**±0.003
Insula	**0.022**±0.003	**0.019**±0.004	**0.023** ± 0.003	**0.023**±0.002	**0.021**±0.036	**0.018**±0.003
Basal ganglia	**0.037**±0.011	**0.036**±0.012	**0.042** ± 0.013	**0.040**±0.010	**0.040**±0.009	**0.043**±0.009
Thalamus	**0.048**±0.006	**0.038**±0.009	**0.047** ± 0.005	**0.045**±0.003	**0.046**±0.010	**0.039**±0.005
Cerebellum	**0.067**±0.019	**0.056**±0.012	**0.067 ±** 0.015	**0.067**±0.002	**0.062**±0.015	**0.060**±0.013

For each group of patients (PPA and MCI), the estimates of both the baseline scan (scan 1) and the scan after treatment with galantamine (scan 2) are displayed. In case of the HC, test- retest values are displayed with scan 1 and 2 respectively the baseline- and repeat scan. +Hippocampus and amygdala. Abbreviations: 2T3k+V_b^{cor} model= two-tissue three-rate constant model including a plasma fraction with a plasma input corrected for metabolites; PPA= primary progressive aphasia; HC= healthy controls and MCI= mild cognitive impairment.

The change in k_3 values when comparing scan 1 vs. 2 differed depending on the VOI and the individual subject that was studied. Figure 3.12 displays for the frontal superior orbital lobe VOI at both the left and right hemisphere (figure 3.12A and B respectively) representative changes in k_3 values before and after treatment in the patient groups, whereas for the HC test-retest values are shown (figure 3.12).

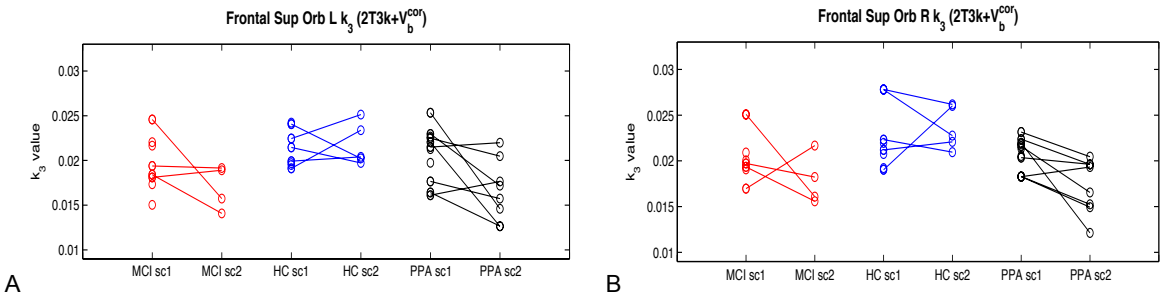

Figure 3.12 Change in k_3 values from scan 1 to scan 2 in all three subgroups using the 2T3k+V_b^{cor} model. Only subjects with two scans available are displayed. The Y-axis represents the values for k_3 (min^{-1}) **A.** The frontal superior orbital lobe, left hemisphere. **B**. The frontal superior orbital lobe, right hemisphere. Abbreviations: 2T3k+V_b^{cor} model= two-tissue three-rate constant model including a plasma fraction with a plasma input corrected for metabolites; MCI= mild cognitive impairment; HC= healthy controls; PPA= primary progressive aphasia; sc1= scan 1 and sc2= scan 2.

The k_3 values of the baseline scans from the HC did not significantly differ from the baseline PPA k_3 estimates. This was true for all VOIs, except for four subregions that are part of the frontal cortex as displayed in table 3.6. When comparing the HC with the MCI patient group, additional VOIs showed at baseline significant different k_3 estimates (table 3.6). The parietal cortex was the cortical region with the highest amount of subregions (5/12) with significant differences between the MCI and the HC k_3 values.

Comparison of the differences in k_3 values from scans 2 and 1 between the HC and patient groups was performed using both absolute (k_3 scan2- k_3 scan1) and relative [(k_3 scan2- k_3 scan1)/ k_3 scan1] differences. These two different approaches gave rise to a shift in results towards more VOIs with significant k_3 differences in case of the relative difference, as displayed in table 3.6. Comparing the relative differences between the control group and the patient groups led to significant different k_3 changes in almost all cortical regions, including the hippocampus, whereas comparing the absolute differences obtained less significant cerebral VOIs (table 3.6).

Next to the comparison between HC and patients, within-group analyses were performed. The results of the analyses are summarized in table 3.7. Test-retest k_3 values of the HC did not show any significant difference, except for two regions i.e. the right amygdala (paired t-test, p_{FDR}=0.048) and pallidum (paired t-test, p_{FDR}=0.045). For the PPA patient group almost all cortical regions showed significant differences after treatment with galantamine.

Table 3.6 Number of VOIs per region with k_3 changes between HC and the patient groups (PPA[a] and MCI[b]) estimated using the 2T3k+V_b^{cor} model: three different levels of comparison.

Brain region	Baseline k_3		Absolute k_3 difference (scan 2 - scan 1)		Relative k_3 difference [(scan 2- scan1)/scan1]	
	PPA vs. HC	MCI vs. HC	PPA vs. HC	MCI vs. HC	PPA vs. HC	MCI vs. HC
Frontal cortex	04/30	08/30	21/30	01/30	28/30	all
Temporal cortex	/	03/12	02/12	01/12	10/12	10/12
Parietal cortex	/	05/12	09/12	06/12	all	all
Occipital cortex	/	01/14	11/14	02/14	11/14	11/14
Hippocampus+	/	/	03/06	02/06	03/06	03/06
Cingulum	/	03/06	04/06	01/06	all	all
Insula	/	/	/	/	all	all
Basal ganglia	/	01/06	/	/	05/06	/
Thalamus	/	/	01/02	/	01/02	01/02
Cerebellum	/	02/26	05/26	02/26	17/26	02/26

Data were analyzed using unpaired t-tests. A statistical test was performed for every VOI of the AAL atlas. The symbol "/" designates that none of the VOIs within that regions showed significant differences. For each subgroup the number of VOIs (per brain region) with significant differences in k_3 values between both groups are displayed. The symbol "/" and term "all" indicate that respectively no and all VOIs within that region showed significance. +Hippocampus and amygdala. Abbreviations: VOI= volume of interest; 2T3k+V_b^{cor} model= two-tissue three-rate constant model including a plasma fraction with a plasma input corrected for metabolites; PPA= primary progressive aphasia; HC= healthy controls and MCI= mild cognitive impairment;

[a]for baseline: p_{FDR}= 0.0489, absolute difference: p_{FDR}= 0.0478 and relative difference: p_{FDR}= 0.0446
[b]for baseline: p_{FDR}= 0.0477, absolute difference: p_{FDR}= 0.0455 and relative difference: p_{FDR}= 0.0432

Table 3.7 Number of VOIs with significant k_3 differences between scan 2 and scan 1 in all three groups using the 2T3k+V_b^{cor} model.

Brain region	PPA[a]	HC[b]	MCI[c]
Frontal cortex	26/30	/	03/30
Temporal cortex	all	/	01/12
Parietal cortex	all	/	03/12
Occipital cortex	all	/	01/14
Hippocampus+	all	1/6	/
Cingulum	04/06	/	01/06
Insula	02/02	/	/
Basal ganglia	01/06	1/6	01/06
Thalamus	/	/	/
Cerebellum	07/26	/	01/26

Data were analyzed using paired t-tests. A statistical test was performed for every VOI of the AAL atlas. For each subgroup the number of VOIs (per brain region) with significant differences in k_3 values between the first and second scan are showed. The symbol "/" and term "all" indicate that respectively no and all VOIs within that region showed significance. +Hippocampus and amygdala. Abbreviations: VOI= volume of interest; 2T3k+V_b^{cor} model= two-tissue three-rate constant model including a plasma fraction with a plasma input corrected for metabolites; PPA= primary progressive aphasia; HC= healthy controls and MCI= mild cognitive impairment. [a]p_{FDR}= 0.0485; [b]p_{FDR}= 0.0478; [c]p_{FDR}= 0.0462.

4. Discussion

The central cholinergic system plays an important role in memory, attention and other cognitive functions (15, 17, 19, 40, 97, 98). Disruption of cholinergic signaling in the cortex is consistently observed in distinct types of degenerative diseases, including both dementing and non-dementing disorders (9). To assess integrity of the cholinergic function, acetylcholinesterase (AchE) has been proven to be a good marker (29). The activity of this enzyme has been studied in vivo using brain-PET imaging of an Ach-analogue tracer in combination with kinetic modeling. The standard method that is used for quantification of AchE is the two-tissue three-rate constant (2T3k) model, a compartmental model of which the rate constant k_3 provides an index for AchE activity (3, 4, 83, 84). In order to remove the need for arterial sampling in compartmental modeling, non-invasive alternatives for AchE quantification were proposed i.e. reference method and shape analysis (85, 87, 90). We tested with the radiotracer 1-[^{11}C]Methylpiperidin-4yl propionate (PMP) the invasive and non-invasive models at multiple levels and this in three different groups of subjects: healthy controls (HC), mild cognitive impairment (MCI) and primary progressive aphasia (PPA) patients.

The major topics in this study can be divided into four consecutive parts. First of all we searched for the fitting function that corrected best for plasma metabolites, an essential requirement to obtain an accurate input for the kinetic model. Secondly, we checked the irreversibility of PMP and we searched for the optimal compartmental model of PMP in the dataset of this study. Thirdly, we examined whether non-invasive analyses could be reliable alternatives. Finally, we investigated the ability to pick up differences in AchE activity both between HC and patients (MCI and PPA) as well as before and after treatment with the cholinesterase inhibitor (ChE-I) galantamine in patients.

To evaluate the first aim of this study i.e. finding the best function to fit the authentic PMP tracer fraction of our data, both Akaiki criteria[95] (AIC) and Schwarz criteria[96] (SC) were used. Five types of fitting functions were assessed (94). Of these functions, the Hill function came out as the best method to correct the plasma input function for the presence of metabolites in case of inclusion of all plasma samples. This was true for the majority of the cases (37 out of 47) and across all three subject groups. The search for a good fitting function is essential since small errors within metabolite correction (MBC) can cause significant errors in the fitted parameters of the model. In addition, fitting is required because only a limited number of metabolite samples are available. Therefore the use of a proper fitting function is advantageous in two ways 1) it avoids additional noise to the final input function 2) it gives an intact fraction curve continuous over time by interpolating few

metabolite measures (99). The reason for the need to apply MBC is that metabolized tracer molecules form no part of the tracer supply from the blood to the brain tissue, at least if it assumed that crossing the blood brain barrier is not possible (73). The input of the 2T3k model is the authentic tracer concentration in the plasma over the total PET scan session. The PMP input function from our data using the Hill function for MBC was in relatively good agreement with that of previous studies with the same tracer (4, 87). Again a low tail indicating little recirculation of the PMP tracer characterized the plasma input function (see figure 2.4). After approximately 30 min, the authentic tracer concentration dropped to below 10%.

The short half-life of carbon-11 (^{11}C) i.e. ± 20 min causes late plasma samples to be less reliable due to the low number of radioactive counts lefts (69, 100). Therefore we additionally studied the case where the late samples were removed from the analysis. So, in order to analyze the influence from the choice of MBC analysis on the estimates of AchE activity, sampling over the total scan time was compared with sampling up to 40 min. Statistical testing showed significant differences in k_3 values across all scans and VOIs, except in one VOI at the cerebellum. Exploratory data showed, using AIC and SC, that MBC with inclusion of all measured samples obtained consistently the best fit. This was observed in both the PPA and HC subgroups whereas for the MCI scans, the choice of best fit for MBC was equally divided. For PET research in general we can state that until now the importance of choosing a proper method for metabolite correction is underestimated.

Following the metabolite analysis, the behavior of PMP was examined. The irreversible character of PMP was confirmed in this study by comparing the irreversible vs. the reversible two-tissue compartmental model. Next to the lower AIC and SC values for the irreversible model in most of the scans and VOIs, the low cortical k_4 values estimated by the reversible 2T4k+V_b^{cor} model further confirmed the irreversible character of PMP. To our knowledge it is the first time that the PMP irreversibility is demonstrated. Most of the previous PET studies for AchE quantification used the tracer 1-[^{11}C]Methylpiperidin-4-yl acetate (AMP) (3, 82, 85, 90, 101, 102). AMP is another Ach-analogue tracer with higher specificity for Ach and a higher hydrolysis rate but with less reliable estimates of the AchE activity in regions with high activity than PMP (32). For the AMP tracer, it was already verified to be irreversible (82). On the other hand for PMP it was always assumed being irreversible because of the hydrophilic nature of its metabolite and the plateau of its brain TAC but never proven to be (82).

The PMP tracer is quite unique in its kind. In general a brain-PET radioligand is considered “ideal” if no tracer metabolites accumulate in the brain (103). Typically, metabolites formed behind the blood brain barrier disturb the specific PET signal because their radioactive signal

contributes to the tissue PET signal but is not of relevance (104). For the PMP tracer, it is different because the metabolites of PMP provide the parameter of interest i.e. AchE activity. After hydrolysis of PMP by the enzyme AchE the tracer metabolite is trapped, which is assumed to render it irreversible. So it is the activity of AchE that causes the metabolites to be retained locally. The metabolites on their turn provide the measurement of the AchE distribution and the quantification of AchE action using PET, the PMP tracer and an appropriate model. If for some reason trapping would be avoided and/or reversed, the specificity of the tracer signal would get contaminated.

In addition to the irreversible character of the PMP tracer, we also found out that inclusion of the plasma fraction (V_b) as an additional parameter gave rise to the best model for kinetic analysis of PMP. For the irreversible 2T3k model, all previous brain-PET studies of AchE activity in humans assumed that either V_b was negligible, either it was on average 0.05 (3, 4, 82, 87, 88). Therefore we tested three subtypes for each of the two main model types i.e. the 2T3k model or the reversible two-tissue four-rate constant (2T4k) model. Each subtype included a certain variant of V_b: 1) V_b=0, 2) V_b with metabolite-corrected plasma input as a measure for the vascular pool (V_b^{cor}) and 3) V_b with metabolite-uncorrected plasma input as a measure for the vascular pool (V_b^{uncor}). Among all 116 VOIs of every scan analyzed in this study, in 91 VOIs the 2T3k+V_b^{cor} model came out as the best model using AIC and SC. For the remaining 25 VOIs, the reversible variant 2T4k+V_b^{cor} was in general the model that described best the kinetics of PMP within these specific volumes of the brain. Evaluation turned out that those 25 VOIs are part of brain regions with very high hydrolysis such as the cerebellum, thalamus and basal ganglia. The model 2T4k+V_b^{cor} denotes reversibility of the PMP tracer, implicating that inclusion of the rate constant k_4 improved the description of the tracer's behavior within these particular brain regions. In addition, it also designates that the model choice for the PMP tracer is region-dependent.

In general, the objective is to find a kinetic model that suits best in most of the cerebral regions. Both postmortem and in vivo studies demonstrated consistently in the cerebellum and the striatum, which is part of the basal ganglia, the high activity of AchE. This feature, observed in our study as well, produces the large range of AchE activities present in the human brain (3, 82, 85, 87, 105). A large range of trapping rates render it difficult to obtain accurate estimates of regional k_3 values in all regions of the brain (4, 105). Therefore, the large differences in k_3 values between the cortical and high hydrolysis regions are probably the cause of the fact that the 2T3k+V_b^{cor} model, which described best the data in most brain regions, did not fit well for the regions with the highest AchE activity. Since in the pathology of dementia the regions of interest concern the cortical lobes, consistency of a best model in the cortical area is most important and was fulfilled in this study.

Referring to the low COVs, most likely reliable k_3 estimates were obtained for the cortical regions in HC with the 2T3k+V_b^{cor} model. Indeed, COV was next to test-retest values used as one of the indicators for reliability of parameter estimations. On the contrary for the cortical regions, which have low to moderate k_3 values, estimates became considerably less precise with increased AchE activity. This was in line with previous studies where the brain regions with the highest hydrolysis rate such as striatum and/or cerebellum did not yield reliable estimates for k_3 using the standard PMP analysis (4, 83, 87). The k_3 estimates of high hydrolysis regions are known to not correspond with necropsy data (105). The reason that regions with high hydrolysis obtain larger COV values is owed to the flow-limitation effect (4). Here, accumulation of metabolites in the brain is dependent on primarily the tracer transport and not our parameter of interest i.e. the rate of AchE hydrolysis. As a consequence, the sensitivity to changes in AchE activity is low resulting in a low reliability for k_3 estimation. But even for high hydrolysis regions our study obtained again lower COVs as compared to some previous PMP studies (83, 87). The COV for the k_3 values of the thalamus (9,8%) was much lower than previously observed in the study of Sato et al.[87] (17%) but for the basal ganglia a similar COV (29%) was observed. For the cerebellum we obtained a lower value for COV (22,6%) than observed by Kuhl et al.[83] (37%) but slightly higher as compared to Sato et al. [87] (17%).

Within the cortical regions and using the 2T3k+V_b^{cor} model, we obtained systematically lower COVs and k_3 values in HC as compared to previous studies quantifying AchE using PMP (4, 83, 87). COV is here, next to one of the indicators of reliability, first of all a measure for the variation in k_3 values across the HC relative to their mean. In general three major sources of variability are supposed to regulate the COV value for a parameter across a group of subjects 1) statistical imprecision, 2) methodological bias and error and 3) true inter-subject biological variability (4). Inter-subject biological difference is a factor of variability that is constant. It is independent of the method applied to model the tracer's kinetics. The two others forms of variability on the other hand do depend on the model and acquisition of the data. In our analysis, it is important to emphasize that the COV of our study had a supplementary source of variability i.e. the variability across the VOIs associated with each brain region (for the subset of VOIs per region see table S-II in the supplementary material). So when interpreting the results both the variability across subjects and VOIs should be considered. Nevertheless, the novel introduced 2T3k+V_b^{cor} subtype was observed in our study to obtain in the cortical regions lower COVs than in previous PMP studies with the standard 2T3k model (83, 87). This might indicate that the use of the 2T3k+V_b^{cor} model improved the PMP analysis. As a consequence inclusion of V_b might probably be more important than previously considered.

Other options explaining the lower COV- and k_3 values in our study might not be overseen. Another explanation might be the difference in included brain tissue. In our study we performed segmentation of the MRI scan to include only grey matter (GM) in the VOIs for the kinetic analysis. It is plausible, although not mentioned, that those previous studies executed the analysis including the total brain tissue i.e. cerebrospinal fluid, GM and white matter (WM). Assessing the total tissue versus only the GM might explain the higher versus lower values estimated in our study. A preliminary study, in cooperation with the Radiology & Nuclear Medicine department of the VUmc Amsterdam, showed that considering both GM and WM obtained higher k_3 values as compared to inclusion of only the GM brain tissue. Since it is known that AchE is present both at the synapse as well as in the axons, adding WM might indeed contribute to higher k_3 values (31, 106). The use of segmentation in this study seemed a logical methodology since the cholinergic cell bodies, which lie in the GM and not the nerve fibers, which are part of the WM tissue, are of interest. Next to the brain tissue under investigation, dissimilarity in the constitution of the subject group might partly explain the relative lower COVs and k_3 values in this study as compared to previous studies. But with regard to the effect of age on the k_3 value, opposing results were obtained. In PET studies with PMP, Sato et al. [87] observed age-associated changes in the normal k_3 values whereas Kilbourn et al. [80] did not, strengthened by the postmortem results of Perry et al. [80, 107]. Next to the previous PMP studies, the in vivo studies for the quantification of AchE that used AMP as radiotracer estimated even higher mean values for k_3 (3, 85, 88, 90). This difference might be explained by the tracer difference as the AMP tracer is known being hydrolyzed three to four times faster than PMP (4, 81). Since the model parameter k_3 is determined by both the AchE concentration and the $k_{hydrolysis}$, which is defined by a combination of two serial processes 1) binding and 2) effective rate of hydrolysis, a different binding specificity might alter the k_3 value (4).

After having demonstrated the best invasive model for kinetic analysis of PMP i.e. the 2T3k+V_b^{cor} model, our third aim was to compare in HC this model with the non- invasive alternatives: reference method (REF) and shape analysis (SA) (4, 90, 91). We obtained a weak and moderate positive correlation with correlation coefficients of 0.28 and 0.40 for respectively the REF and SA. However, previous PET studies with an Ach-analogue yielded for both invasive methods much more favorable results. The study by Koeppe et al.[4], which first proposed the SA method with PMP, presented it as a reliable method for the estimation of AchE activity in healthy subjects. Sato et al.[87] confirmed this result by the observation of a high correlation (r=0.89) between the k_3 estimates of the SA and the standard 2T3k model. In addition they showed that the variability in cortical k_3 estimates using the standard model was almost identical for the SA, whereas in our study the variability in k_3 values was higher for the SA as compared to the 2T3k+V_b^{cor} model. The opposing findings can have different possible

explanations. Both the methodology and/or the difference in VOI definition might be plausible reasons for the discrepancy in outcome. Simulation studies performed by Tanaka et al.[88], which developed an optimized protocol for the SA but using the AMP tracer, demonstrated that SA is sensitive to PET data errors in later scan frames, in particular the last scan frame (88). The reason for the larger bias at later scan frames is assigned to the zero input assumption of the SA method. The latter requires that at the end of the scan session no authentic tracer is present in the brain tissue (4). Therefore the final value of the measured brain TAC is of critical importance. The total accumulation of metabolites that is calculated in the final frame must equal the final measured PET concentration, thereby implicating the importance of scan duration, which was demonstrated by Tanaka et al. (88). Our scan time period differed from the scan time used by Koeppe et al.[4] (80 min vs. 60 min our study). Probably the total scan time of 60 min was not sufficient to fulfill the zero input assumption of the SA and indeed at the end of our study still some fraction of authentic tracer was present. In other words not all authentic tracer molecules in the brain tissue were metabolized at the final PET frame. In general for kinetic modeling the accuracy of model parameter estimates depends on the validity of assumptions made by the model. So the limited ability of the SA to obtain reliable k_3 estimates might be clarified by violation of the zero input assumption in our study. But before conclusions can be drawn, further investigation on the importance of scan time is needed to unravel the contribution to the discrepancy in results. Next to this difference in methodology, the delineation and segmentation of the regions of interest should be compared and considered.

According as with the SA, also for the REF contrasting results were obtained as compared to previous studies. Whereas in studies with AMP a good correlation (r=0.89) was observed between REF and the standard method, we had a correlation coefficient of 0.28 (85, 87, 90). Difference in tracer's use might cause a difference in k_3 estimates because AMP and PMP are both Ach-analogue tracers but the kinetic properties differ. The hydrolysis rate of AMP is much higher, so is its specificity for the enzyme AchE. Therefore Sato et al.[87] investigated the applicability of the two available reference tissue-based analyses for the PMP tracer (85, 90). Their analysis revealed that both methods, originally developed for AMP, could be used with the PMP tracer using the striatum as the reference region. They even concluded that both these non-invasive kinetic analyses could be used to track regions with altered AchE activity in patients as compared to HC. In addition they observed the COVs of the non-invasive methods to be comparable to the COVs of the standard 2T3k method. Our study on the contrary had larger COVs for the non-invasive method. We obtained a large variability for the k_3 values of HC and large amplitude for test-retest using the REF, which was not the case when applying the 2T3k+V_b^{cor} model.

For the analysis of the REF, such as with the SA, violation of a model assumption could be a reason for the contrasting results with other studies. The REF was developed based on studies with AMP, which is as stated already, a tracer with a hydrolysis rate three to four times higher than PMP (4, 81). In the REF a region with a very high AchE activity is used as a reference that act as a "biological integrator" of the input (91). Therefore the assumption that the rate constant k_2 is much lower than k_3 must be fulfilled. Since our tracer is not AMP but the other Ach-analogue tracer PMP, which has a much lower hydrolysis rate, this assumption might be violated. We used the putamen, a structure of the striatum, as reference region according to the study of Zundorf et al.[91] of which we applied the REF calculation method. Following the kinetic analysis we observed that the cerebellum was the region with highest AchE activity in our study and not the putamen. For Sato and colleagues[87], which did obtained with PMP reasonable results using the REF, the striatum as the reference region obtained the highest hydrolysis rate. Therefore, examining whether the cerebellum as the reference region for our data would give better estimates for k_3 using REF should be a logical next step.

Since the Pearson correlation analysis measures the strength of association but not the agreement, we additionally applied a Bland-Altman analysis (figure 3.8B and 3.9B). This allowed investigating by comparison the ability of the non-invasive methods REF and SA to replace the invasive 2T3k+V_b^{cor} model. A trend was observed with larger differences in k_3 values between the non-invasive methods and the invasive model if the mean k_3 increased. The large measured discrepancy and wide percentiles for the REF suggest this method to be unsatisfactory to replace the invasive 2T3k+V_b^{cor} model. For the SA a better result with the Bland-Altman analysis was obtained, which was in agreement with the lower amplitude for test-retest and lower variability of k_3 values (figure 3.10) as compared to REF. Nevertheless, the SA was probably still not suitable enough the replace properly the 2T3k+V_b^{cor} model.

The last part of this study investigated exploratory the power of the PMP tracer and the 2T3k+V_b^{cor} model to pick up differences in AchE activity between the controls and the patient groups i.e. patients with MCI and PPA. At baseline we observed only a few VOIs with significant differences between the k_3 values of the HC vs. the patient groups. If the absolute differences in baseline and follow-up k_3 values (k_3 scan 1- k_3 scan 2) were considered, then the patient groups showed much more VOIs with significant lower k_3 differences. Interestingly, applying the relative difference [(k_3 scan 2- k_3 scan1)/ k_3 scan1] led to most VOIs in which these differences were significant different between patients and HC. Indeed, when comparing the relative difference in k_3 values of HC vs. patients, the number of significant VOIs was strongly increased as compared to the absolute difference. The reason of this observation might be explained by the nature of the k_3 parameter. Since the values for

k_3 are rather small, the difference between the k_3 values of scan 2 and 1 will be even smaller. In case this small difference is divided by the k_3 values of the first scan, the resulting relative difference will obtain a higher value.

We can state that with the PMP tracer and 2T3k+V_b^{cor} model significant changes in k_3 values between controls and patients were detected in almost all VOIs if the alterations from the first to the second scan were considered. At baseline on the contrary, very few VOIs were observed to show significant different k_3 values between HC and the patients groups. This might be an indication of a still intact cholinergic system in the MCI and PPA patients (28-29). Whether or not the changes induced after intake of galantamine by the patients are of clinical relevance require additional analyses. Moreover, it is important to consider the fact that controls besides absence of drug therapy also differ from the patient groups in that no brain pathology is present. For now we did not evaluate the inhibiting effect of the drug on the specific cognitive function of the patient groups. A good approach would be to first look if the patient groups after treatment showed improved scores for the cognitive tests. In case an improvement was present, we would correlate the scores from the cognitive tests with AchE activity, both before and after treatment. Previously, the association between cholinergic activity and cognitive function was confirmed in brain biopsy studies of healthy and demented subjects using choline acetyltransferase (ChAT) as cholinergic marker (108-111). Since AchE is known to map cholinergic activity in good accordance with ChAT, we expect the same association to be present (112).

In our study, the correlation between an elevated and/or stabilized cognition after treatment with galantamine and a reduced AchE activity would indicate a beneficial effect of the drug in the PPA patients. But for the group of MCI patients it will be more challenging to evaluate the true effect of galantamine. Whereas PPA is always a progressive syndrome, this is not the case for the MCI syndrome. Patients with MCI are at increased risk to develop AD but not all will eventually develop dementia (51). Within 3 years of diagnosis, 19-50% of the total group MCI patients will develop to AD, whereas the remaining part reverts to normal cognition or can stabilize (5, 51). Our study performed the follow-up scan on average 1 year after the start with drug therapy. So potential improvements in cognitive function of the MCI patients after that time period might be ascribed to disease progression and not the action of the drug. However, since further cognitive decline is more likely among MCI patients with already memory problems, our MCI dataset with solely amnestic MCI patients might not encounter that problem (56).

Heterogeneity in the MCI syndrome might also be one of the reasons for the previous observed lack of benefit from the ChE-Is in clinical trials with MCI patients. There is

consistent evidence from reviews that ChE-Is are not efficacious to treat MCI (58-60). A later review in 2012 using meta-analysis confirmed these results and stated that there is essentially no effect of ChE-Is on the scores of cognitive tests performed by MCI patients (60). Nevertheless these results need to be interpreted with caution because differences in both disease outcome of MCI as the criteria for diagnosis of this syndrome make comparison across clinical trials difficult (5, 56). Therefore, further research is needed where standardized protocols are used to diagnose and to classify MCI patients into the different subtypes. It might be that only certain subtypes of MCI benefit from treatment with a ChE-I. Hence in the future it seems valuable to compare and evaluate studies with not a mixture but the same subtypes of MCI. Our study demonstrates the first step in that direction. We solely investigated the amnestic subtype of MCI (5, 6, 52, 57). In this MCI subgroup we observed a reduction in AchE activity after treatment with galantamine. However, to evaluate the significance of this reduction, more studies are necessary.

Conversely to the negative results of clinical trials in MCI patients with ChE-Is, investigation of the cholinergic system in this patient group is worth pursuing. In 2014, The National Institute on Aging-Alzheimer's Association[51] suggested that AD should be optimally treated at a 'pre-symptomatic' or 'preclinical' stage before the occurrence of significant cognitive dysfunction. As the MCI patients are considered a possible transition stage from normal function to AD, the study of ChE-Is in this patient group might assist to further unravel the etiology of AD, which is until now still unknown. Next to the search for the etiology and the evaluation of pharmaceutical agents in dementia patients, PET kinetic modeling with PMP could also play a role in classifying the MCI patients into the distinct subgroups. If by using longitudinal studies we would observe that only the MCI subgroup with AD outcome react to the drug, the first objective method for subtype prediction could be developed.

The few differences in AchE activity at baseline between HC and the MCI patient group suggest the cholinergic function not to be an early predictive marker for dementia. So far the findings in MCI patients regarding the predictive role of the cholinergic system for dementia are opposing and should be considered preliminary. Postmortem studies observed preservation of the cholinergic function and one biopsy study even found a significant upregulation of the ChAT marker in MCI (68, 113, 114). The in vivo studies that measured AchE activity in MCI patients show controversial results as well. Herholz et al.[115] suggested the reduction of cortical AchE activity to be related with impending AD in MCI but stated later on that additional research is needed (116). Several years later, Haense et al.[117], another PET study but with a larger sample size, again proposed the cholinergic dysfunction as an early hallmark of AD. Rinne et al.[118] by contrast concluded that the power of AchE measurement as an early AD marker is limited. As a consequence, additional and larger

studies with MCI patients are needed to assess the value of in vivo quantification of AchE activity in detecting a possible non-dementia phase of AD.

Next to investigation in MCI patients, we also studied the AchE activity in PPA patients. A significant decrease of AchE activity after treatment with galantamine was observed in the PPA group of this study. All VOIs of the four lobes at the cortex (except four VOIs at the frontal cortex) showed significant reduced k_3 values after treatment with galantamine. At present no drug therapy is available for this specific group of patients. The same as with the MCI group, conductance of several clinical trials with pharmacological agents in PPA patients lack any proof of efficacy (119, 120). Development of new drugs and evaluation of existing drugs has been impeded by the absence of a standardized methodology to monitor progression of this disorder (121).

Our study shows promise that quantification of AchE activity might be used to assess the effect of a ChE-I type in PPA patients. A placebo-controlled study with galantamine in PPA patients also showed a treatment effect ($p=0.0009$) but the effect was declined after correction for multiple comparisons (120). In addition, they observed a trend that indicated the stabilization of language score for PPA that were treated, whereas the placebo group showed deterioration. The consequence of the inhibiting drug effect observed in PPA patients of our study needs further investigation. Imaging drug effects and relating them to cognitive improvement will offer an approach to monitor the causal effects of galantamine in PPA patients and to identify patients who are most likely to respond to treatment.

Possible limitations of this study require consideration when interpreting the results. A first limitation might be present due to the size of the three subject groups. In total we obtained a relatively large number of scans ($n=47$) but the division into three groups (HC, MCI and PPA) as well as the division into baseline vs. follow-up scan render each individual (sub)-group relatively small. The MBC analysis, the analysis about the irreversible character of PMP and the best model to describes its kinetics will likely not suffer from this limitation since here the total set of scans was used. On the contrary the between-group analyses (patients vs. HC) and the within-group analyses (baseline vs. follow-up scan) may encounter a limitation. Therefore these results should be considered exploratory and studies with a larger sample size are necessary to make further conclusions. In addition, only plasma samples were analyzed in this study. Whole blood measurements were not performed and as a consequence the blood/plasma ratio could not be calculated. This might possibly affect the value of the fraction of the vascular pool in the brain. A possible difference in tracer concentration between plasma and whole blood can lead to a different blood volume fraction, depending on the characteristics of tracer.

We can conclude that the methodology for MBC is a determining factor for the estimation of AchE activity in the human brain using the PMP tracer. To quantify in vivo AchE activity with PMP, the 2T3k model including the plasma fraction and using the plasma input function corrected for metabolites as a measure for the vascular pool in the brain (2T3k+V_b^{cor}) is the best model in the regions of interest for dementia i.e. the cortical regions and limbic structures of the human brain. However, the non-invasive alternatives REF and SA are not recommended for AchE quantification, even though they are attractive to implement. Furthermore, it was shown that PMP in combination with the 2T3k+V_b^{cor} model is able to pick up significant changes in AchE activity at VOI-level after treatment with galantamine in the MCI and PPA groups, as compared to the HC.

References

1. Davies P, Maloney AJ. Selective loss of central cholinergic neurons in Alzheimer's disease. Lancet. 1976; 2(8000):1403.

2. Irie T, Fukushi K Fau - Akimoto Y, Akimoto Y Fau - Tamagami H, Tamagami H Fau - Nozaki T, Nozaki T. Design and evaluation of radioactive acetylcholine analogs for mapping brain acetylcholinesterase (AchE) in vivo. Nucl Med Biol. 1994;21(6):801-8.

3. Iyo M, Namba H, Fukushi K, Shinotoh H, Nagatsuka S, Suhara T, et al. Measurement of acetylcholinesterase by positron emission tomography in the brains of healthy controls and patients with Alzheimer's disease. The Lancet. 1997;349(9068):1805-9.

4. Koeppe RA, Frey KA, Snyder SE, Meyer P, Kilbourn MR, Kuhl DE. Kinetic modeling of N-[11C]methylpiperidin-4-yl propionate: alternatives for analysis of an irreversible positron emission tomography trace for measurement of acetylcholinesterase activity in human brain. J Cereb Blood Flow Metab. 1999;19(10):1150-63.

5. Gauthier S, Reisberg B, Zaudig M, Petersen RC, Ritchie K, Broich K, et al. Mild cognitive impairment. The Lancet. 2006;367(9518):1262-70.

6. Petersen RC, Doody R, Kurz A, Mohs RC, Morris JC, Rabins PV, et al. Current concepts in mild cognitive impairment. Archives of neurology. 2001;58(12):1985-92.

7. Mesulam MM, Rogalski EJ, Wieneke C, Hurley RS, Geula C, Bigio EH, et al. Primary progressive aphasia and the evolving neurology of the language network. Nature reviews Neurology. 2014;10(10):554-69.

8. Karczmar AG. Exploring the Vertebrate Central Cholinergic Nervous System. Dordrecht : Springer; 2007. [cited 2015 May 19]. Available from SpringerLink (online service).

9. Schliebs R, Arendt T. The significance of the cholinergic system in the brain during aging and in Alzheimer's disease. J Neural Transm. 2006;113(11):1625-44.

10. Siegel GJ, Agranoff BW, Gavulic LM. Basic neurochemistry : molecular, cellular, and medical aspects. 6th ed. Philadelphia: Lippincott Williams and Wilkins; 1999.

11. Mufson EJ, Kordower JH. Cholinergic basal forebrain systems in the primate central nervous system: anatomy, connectivity, neurochemistry,aging, dementia and experimental therapeutics. In: Hof PR, Moobs CV, editors. Functional Neurobiology of Aging. San Diego: Academic Press; 2000. Chapter 19; p. 243–76.

12. Mesulam MM, Mash D, Hersh L, Bothwell M, Geula C. Cholinergic innervation of the human striatum, globus pallidus, subthalamic nucleus, substantia nigra, and red nucleus. J Comp Neurol. 1992;323(2):252-68.

13. Mesulam MM, Geula C. Nucleus basalis (Ch4) and cortical cholinergic innervation in the human brain: observations based on the distribution of acetylcholinesterase and choline acetyltransferase. J Comp Neurol. 1988;275(2):216-40.

14. Mesulam MM. Structure and Function of Cholinergic Pathways in the Cerebral Cortex, Limbic System, Basal Ganglia, and Thalamus of the Human Brain [Internet]. 2000 [updated 2015 May 19; cited 2015 May 19]. Available from: http://www.acnp.org/g4/GN401000012/Default.htm.

15. Sarter M, Bruno JP, Givens B. Attentional functions of cortical cholinergic inputs: what does it mean for learning and memory? Neurobiol Learn Mem. 2003;80(3):245-56.

16. Luiten P, Nyakas C, Eisel U, van der Zee E. Aging of the Brain. In: Pfaff D, editor. Neuroscience in the 21st Century. New York: Springer; 2013. Chapter 84; p. 2239-72.

17. Gold PE. Acetylcholine modulation of neural systems involved in learning and memory. Neurobiol Learn Mem. 2003;80(3):194-210.

18. Micheau J, Marighetto A. Acetylcholine and memory: A long, complex and chaotic but still living relationship. Behavioural Brain Research. 2011;221(2):424-9.

19. Woolf NJ, Butcher LL. Cholinergic systems mediate action from movement to higher consciousness. Behavioural Brain Research. 2011;221(2):488-98.

20. Purves D, Augustine GJ, Fitzpatrick D. Neuroscience. 5th ed. Sunderland: Sinauer; 2012.

21. Felder CC, Bymaster FP, Ward J, DeLapp N. Therapeutic Opportunities for Muscarinic Receptors in the Central Nervous System. Journal of Medicinal Chemistry. 2000;43(23):4333-53.

22. Dajas-Bailador F, Wonnacott S. Nicotinic acetylcholine receptors and the regulation of neuronal signalling. Trends in Pharmacological Sciences. 2004;25(6):317-24.

23. Kalamida D, Poulas K, Lagoumintzis G, Zouridakis M, Tzartos SJ, Avramopoulou V, et al. Muscle and neuronal nicotinic acetylcholine receptors: Structure, function and pathogenicity. FEBS Journal. 2007;274(15):3799-845.

24. Caulfield MPP. Muscarinic receptors--characterization, coupling and function. Pharmacology & therapeutics. 1993;58(3):319-79.

25. Bear Mark F, Connors BW, Paradiso Michael A. Neuroscience: Exploring the brain. 3rd ed. Philadelpia: Lippincott Williams and Wilkins; 2007.

26. Soreq H, Seidman S. Acetylcholinesterase--new roles for an old actor. Nat Rev Neurosci. 2001;2(4):294-302.

27. Brimijoin S. Molecular forms of acetylcholinesterase in brain, nerve and muscle: Nature, localization and dynamics. Progress in Neurobiology. 1983;21(4):291-322.

28. Schegg KM, Harrington LS, Neilsen S, Zweig RM, Peacock JH. Soluble and membrane-bound forms of brain acetylcholinesterase in Alzheimer's disease. Neurobiol Aging. 1992;13(6):697-704.

29. Wevers A. Localisation of pre- and postsynaptic cholinergic markers in the human brain. Behav Brain Res. 2011;221(2):341-55.

30. Selden NR, Gitelman DR, Salamon-Murayama N, Parrish TB, Mesulam MM. Trajectories of cholinergic pathways within the cerebral hemispheres of the human brain. Brain : a journal of neurology. 1998;121(Pt 12):2249-57.

31. Kása P. The cholinergic systems in brain and spinal cord. Progress in Neurobiology. 1986;26(3):211-72.

32. Bohnen NI, Frey KA. Imaging of cholinergic and monoaminergic neurochemical changes in neurodegenerative disorders. Molecular Imaging and Biology. 2007;9(4):243-57.

33. Perry EK, Perry RH, Blessed G, Tomlinson BE. Necropsy evidence of central cholinergic deficits in senile dementia. Lancet. 1977;1(8004):189.

34. Perry EK, Gibson PH, Blessed G, Perry RH, Tomlinson BE. Neurotransmitter enzyme abnormalities in senile dementia: Choline acetyltransferase and glutamic acid decarboxylase activities in necropsy brain tissue. Journal of the Neurological Sciences. 1977;34(2):247-65.

35. Perry EK, Perry RH, Blessed G, Tomlinson BE. Changes in brain cholinesterases in senile dementia of Alzheimer type. Neuropathol Appl Neurobiol. 1978;4(4):273-7.

36. Whitehouse PJ, Price DL, Struble RG, Clark AW, Coyle JT, Delon MR. Alzheimer's disease and senile dementia: loss of neurons in the basal forebrain. Science. 1982;215(4537):1237-9.

37. Bowen DM, Smith CB, White P, Davison AN. Neurotransmitter-related enzymes and indices of hypoxia in senile dementia and other abiotrophies. Brain. 1976;99(3):459-96.

38. Wilcock GK, Esiri MM, Bowen DM, Smith CCT. Alzheimer's disease: Correlation of cortical choline acetyltransferase activity with the severity of dementia and histological abnormalities. Journal of the Neurological Sciences. 1982;57(2):407-17.

39. Bartus RT, Dean RL, Beer B, Lippa AS. The cholinergic hypothesis of geriatric memory dysfunction. Science. 1982;217(4558):408-14.

40. Bartus RT. On Neurodegenerative Diseases, Models, and Treatment Strategies: Lessons Learned and Lessons Forgotten a Generation Following the Cholinergic Hypothesis. Experimental Neurology. 2000;163(2):495-529.

41. Lane RM, Potkin SG, Enz A. Targeting acetylcholinesterase and butyrylcholinesterase in dementia. Int J Neuropsychopharmacol. 2006;9(1):101-24.

42. Cummings JL. Cholinesterase Inhibitors: A New Class of Psychotropic Compounds. American Journal of Psychiatry. 2000;157(1):4-15.

43. Gauthier S. Advances in the pharmacotherapy of Alzheimer's disease. CMAJ 2002;166(5):616-23.

44. Nygaard HB. Current and Emerging Therapies for Alzheimer’s Disease. Clinical Therapeutics. 2013;35(10):1480-9.

45. Birks J. Cholinesterase inhibitors for Alzheimer's disease. The Cochrane database of systematic reviews. 2006(1):CD005593.

46. Doody RS, Stevens JC, Beck C, Dubinsky RM, Kaye JA, Gwyther L, et al. Practice parameter: Management of dementia (an evidence- based review): Report of the quality standards subcommittee of the American Academy of Neurology. Neurology. 2001;56(9):1154-66.

47. Cummings JL, Cole G. Alzheimer disease. JAMA. 2002;287(18):2335-8.

48. Farlow M. A clinical overview of cholinesterase inhibitors in Alzheimer's disease. Int Psychogeriatr. 2002;14 Suppl 1:93-126.

49. Lemstra AW, Richard E, van Gool WA. Cholinesterase inhibitors in dementia: yes, no, or maybe? Age Ageing. 2007;36(6):625-7.

50. Hardiman O, Doherty CP. Neurodegenerative Disorders: A Clinical Guide. London: Springer; 2011. [cited 2015 May 19]. Available from SpringerLink (online service).

51. Alzheimer’s Association. 2014 Alzheimer's disease facts and figures. Alzheimer's & dementia : The Journal of the Alzheimer's Association. 2014;10(2):e47.

52. Albert MS, DeKosky ST, Dickson D, Dubois B, Feldman HH, Fox NC, et al. The diagnosis of mild cognitive impairment due to Alzheimer's disease: Recommendations from the National Institute on Aging- Alzheimer's Association workgroups on diagnostic guidelines for Alzheimer's disease. Alzheimer's & Dementia: The Journal of the Alzheimer's Association. 2011;7(3):270-9.

53. Terry Jr AV, Buccafusco AV. The cholinergic hypothesis of age and Alzheimer's disease- related cognitive deficits: Recent challenges and their implications for novel drug development. Journal of Pharmacology and Experimental Therapeutics. 2003;306(3):821-7.

54. Sperling RA, Aisen PS, Beckett LA, Bennett DA, Craft S, Fagan AM, et al. Toward defining the preclinical stages of Alzheimer's disease: Recommendations from the National Institute on Aging- Alzheimer's Association workgroups on diagnostic guidelines for Alzheimer's disease. Alzheimer's & Dementia: The Journal of the Alzheimer's Association. 2011;7(3):280-92.

55. Ganguli M, DeKosky ST, Dodge HH, Shen C. Mild cognitive impairment, amnestic type: An epidemiologic study. Neurology. 2004;63(1):115-21.

56. Petersen RC. Mild cognitive impairment as a diagnostic entity. Journal of Internal Medicine. 2004;256(3):183-94.

57. RC. P. Mild cognitive impairment: Aging to Alzheimer's disease. Oxford: Oxford University Press; 2003.

58. Diniz BS, Pinto JA, Gonzaga MLC, Guimarães FM, Gattaz WF, Forlenza OV. To treat or not to treat? A meta-analysis of the use of cholinesterase inhibitors in mild cognitive impairment for delaying progression to Alzheimer's disease. Eur Arch Psychiatry Clin Neurosci. 2009;259(4):248-56.

59. Raschetti R, Albanese E, Vanacore N, Maggini M. Cholinesterase inhibitors in mild cognitive impairment: a systematic review of randomised trials. PLOS Medicine. 2007;4(11):1818-28

60. Russ TC, Morling JR. Cholinesterase inhibitors for mild cognitive impairment. The Cochrane database of systematic reviews. 2012;9:CD009132.

61. Petersen RC, Jack Jr CR. Imaging and biomarkers in early alzheimer's disease and mild cognitive impairment. Clinical Pharmacology and Therapeutics. 2009;86(4):438-41.

62. Matias-Guiu JA, Moreno-Ramos T, García-Ramos R, Porta-Etessam J, Matías-Guiu J, Cabrera-Martín MN, et al. Clinical course of primary progressive aphasia: clinical and FDG- PET patterns. Journal of Neurology. 2014;262(3):570-77.

63. Mesulam MM. Primary progressive aphasia. Ann Neurol. 2001;49(4):425-32.

64. Gorno-Tempini ML, Hillis AE, Weintraub S, Kertesz A, Mendez M, Cappa SF, et al. Classification of primary progressive aphasia and its variants. Neurology. 2011;76(11):1006-14.

65. Wilson SM, Henry ML, Besbris M, Ogar JM, Dronkers NF, Jarrold W, et al. Connected speech production in three variants of primary progressive aphasia. Brain. 2010;133(7):2069-88.

66. Sapolsky D. Monitoring progression of primary progressive aphasia: current approaches and future directions. Neurodegenerative Disease Management. 2011;1(1):43-55.

67. Grothe M, Heinsen H, Teipel S. Cognitive correlates of cholinergic basal forebrain atrophy and associated cortical hypometabolism in mild cognitive impairment. Alzheimer's & Dementia: The Journal of the Alzheimer's Association. 2013; 9(4):P261.

68. Dekosky ST, Ikonomovic MD, Styren SD, Beckett L, Wisniewski S, Bennett DA, et al. Upregulation of choline acetyltransferase activity in hippocampus and frontal cortex of elderly subjects with mild cognitive impairment. Annals of Neurology. 2002;51(2):145-55.

69. Bailey DL, Townsend DW, Valk PE, Maisey MN. Positron emission tomography: basic sciences. New York: Springer; 2005. [cited 2015 May 19]. Available from SpringerLink.

70. Phelps ME, editor. PET: Physics, Instrumentation, and Scanners. New York: Springer; 2006. [cited 2015 May 19]. Available from SpringerLink.

71. Suetens P. Fundamentals of medical imaging. 2nd ed., 4th printing ed. New York: Cambridge university press; 2013.

72. Kim EE, Lee M-C, Inoue T, Wong W-H, editors. Clinical PET and PET/CT: Principles and Applications. 2nd ed. New York: Springer; 2013. [cited 2015 May 19]. Available from SpringerLink.

73. Lammertsma AA. Radioligand studies: imaging and quantitative analysis. European Neuropsychopharmacology. 2002;12(6):513-6.

74. Morris ED, Endres CJ, Schmidt KC, Christian BT, Muzic RF Jr, Fisher RE: Kinetic modeling in positron emission tomography. In: Wermick MN, Aarsvold JN, editors. Emission Tomography: The Fundamentals of PET and SPECT. Oxford: Elsevier Academic Press.; 2014.p 499-540. Chapter 23. [cited 2015 May 19]. Available from ScienceDirect.

75. Dierckx R, Otte A, de Vries E, van Waarde A, Leenders K. PET and SPECT in Neurology. Heidelberg: Springer-Verlag; 2014.

76. Ledder G. Differential equations: a modeling approach. Boston: Boston McGraw-Hill; 2005.

77. Beck JV, Arnold KJ. Parameter estimation in engineering and science. New York: Wiley; 1977.

78. Bergmann SR, Herrero P, Markham J, Weinheimer CJ, Walsh MN. Noninvasive quantitation of myocardial blood flow in human subjects with oxygen- 15- labeled water and positron emission tomography. Journal of the American College of Cardiology. 1989;14(3):639-52.

79. Kaufmann PA, Camici PG. Myocardial blood flow measurement by PET: technical aspects and clinical applications. Journal of nuclear medicine : official publication, Society of Nuclear Medicine. 2005;46(1):75-8.

80. Kilbourn MR, Snyder SE, Sherman PS, Kuhl DE. In vivo studies of acetylcholinesterase activity using a labeled substrate, N-[11C]methylpiperdin-4-yl propionate ([11C]PMP). Synapse. 1996;22(2):123-31.

81. Irie T, Fukushi K, Namba H, Iyo M, Tamagami H, Nagatsuka S, et al. Brain acetylcholinesterase activity: Validation of a PET tracer in a rat model of Alzheimer's disease. J Nucl Med. 1996;37(4):649-55.

82. Namba H, Iyo M, Fukushi K, Shinotoh H, Nagatsuka S, Suhara T, et al. Human cerebral acetylcholinesterase activity measured with positron emission tomography: procedure, normal values and effect of age. Eur J Nucl Med. 1999;26(2):135-43.

83. Kuhl DE, Koeppe RA, Minoshima S, Snyder SE, Ficaro EP, Foster NL, et al. In vivo mapping of cerebral acetylcholinesterase activity in aging and Alzheimer's disease. Neurology. 1999;52(4):691-9.

84. Kilbourn MR, Snyder SE, Sherman PS, Kuhl DE. In vivo studies of acetylcholinesterase activity using a labeled substrate, N-11Cmethylpiperdin- 4- yl propionate (11CPMP). Synapse. 1996;22(2):123-131.

85. Nagatsuka Si S, Fukushi K, Shinotoh H, Namba H, Iyo M, Tanaka N, et al. Kinetic analysis of [(11)C]MP4A using a high-radioactivity brain region that represents an integrated input function for measurement of cerebral acetylcholinesterase activity without arterial blood sampling. J Cereb Blood Flow Metab. 2001;21(11):1354-66.

86. Namba H, Fukushi K, Nagatsuka S-i, Iyo M, Shinotoh H, Tanada S, et al. Positron emission tomography: quantitative measurement of brain acetylcholinesterase activity using radiolabeled substrates. Methods. 2002;27(3):242-50.

87. Sato K, Fukushi K, Shinotoh H, Nagatsuka S, Tanaka N, Aotsuka A, et al. Evaluation of simplified kinetic analyses for measurement of brain acetylcholinesterase activity using N-[11C]Methylpiperidin-4-yl propionate and positron emission tomography. J Cereb Blood Flow Metab. 2004;24(6):600-11.

88. Tanaka N, Fukushi K, Shinotoh H, Nagatsuka S, Namba H, Iyo M, et al. Positron emission tomographic measurement of brain acetylcholinesterase activity using N-[(11)C]methylpiperidin-4-yl acetate without arterial blood sampling: methodology of shape analysis and its diagnostic power for Alzheimer's disease. J Cereb Blood Flow Metab. 2001;21(3):295-306.

89. Namba H, Irie T, Fukushi K, Iyo M. In vivo measurement of acetylcholinesterase activity in the brain with a radioactive acetylcholine analog. Brain Research. 1994;667(2):278-82.

90. Herholz K, Lercher M, Wienhard K, Bauer B, Lenz O, Heiss WD. PET measurement of cerebral acetylcholine esterase activity without blood sampling. Eur J Nucl Med. 2001;28(4):472-7.

91. Zundorf G, Herholz, K., Lercher, M., Wienhard, K.,Bauer, B., Weinsenbach, S., Heiss, W.D. PET functional parametric images of aceylcholine esterase activity without blood sampling. In: Senda M, Kimura Y, Herscovitch P, editors. Brain Imaging using PET. Chapter 7. Boston: Elsevier Academic Press; 2002.

92. Snyder SE, Tluczek L, Jewett DM, Nguyen TB, Kuhl DE, Kilbourn MR. Synthesis of 1-[11c]methylpiperidin-4-yl propionate ([11c]pmp) for in vivo measurements of acetylcholinesterase activity. Nuclear Medicine and Biology. 1998;25(8):751-4.

93. Tzourio- Mazoyer N, Landeau B, Papathanassiou D, Crivello F, Etard O, Delcroix N, et al. Automated anatomical labeling of activations in SPM using a macroscopic anatomical parcellation of the MNI MRI single-subject brain. Neuroimage. 2002;15(1):273-89.

94. Nelissen N, Warwick J and Dupont P. Kinetic Modelling in Human Brain Imaging. In: Hsieh CH, editor. Positron Emission Tomography - Current Clinical and Research Aspects.2012. Chapter 3. Available from: IntechOpen.

95. Akaike H. A new look at the statistical model identification. Automatic Control, IEEE Transactions on. 1974;19(6):716-23.

96. Schwarz G. Estimating the Dimension of a Model. Ann Statist. 1978;6(2):461-4.

97. Woolf NJ. A structural basis for memory storage in mammals. Progress in Neurobiology. 1998;55(1):59-77.

98. Hasselmo M, Sarter M. Modes and Models of Forebrain Cholinergic Neuromodulation of Cognition. Neuropsychopharmacology. 2011;36(1):52-73.

99. Veronese M, Gunn RN, Zamuner S, Bertoldo A. A non- linear mixed effect modelling approach for metabolite correction of the arterial input function in PET studies. Neuroimage. 2013;66:611.

100. Någren K, Halldin C, Rinne J. Radiopharmaceuticals for positron emission tomography investigations of Alzheimer's disease. Eur J Nucl Med Mol Imaging. 2010;37(8):1575-93.

101. Fukushi K, Shinotoh H, Namba H, Iyo M, Tanaka N, Aotsuka A, et al. Kinetic Analysis of [11C]MP4A Using a High-Radioactivity Brain Region That Represents an Integrated Input Function for Measurement of Cerebral Acetylcholinesterase Activity Without Arterial Blood Sampling. Journal of Cerebral Blood Flow and Metabolism. 2001;21(11):1354-66.

102. Herholz K, Bauer B, Wienhard K, Kracht L, Mielke R, Lenz O, et al. In- vivo measurements of regional acetylcholine esterase activity in degenerative dementia: comparison with blood flow and glucose metabolism. J Neural Transm. 2000;107(12):1457-68.

103. Ceccarini J. The cerebral type 1 cannabinoid receptor as modulator in dopaminergic transmission disorders: addiction and psychosis [Phd thesis]. Leuven: KU Leuven university; 2012.

104. Pike VW. PET radiotracers: crossing the blood– brain barrier and surviving metabolism. Trends in Pharmacological Sciences. 2009;30(8):431-40.

105. Atack JR, Perry EK, Bonham JR, Candy JM, Perry RH. Molecular forms of acetylcholinesterase and butyrylcholinesterase in the aged human central nervous system. J Neurochem. 1986;47(1):263-77.

106. Kása P, Rakonczay Z, Gulya K. The cholinergic system in Alzheimer's disease. Progress in Neurobiology. 1997;52(6):511-35.

107. Perry EK, Johnson M, Kerwin JM, Piggott MA, Court JA, Shaw PJ, et al. Convergent cholinergic activities in aging and Alzheimer's disease. Neurobiology of Aging. 1992;13(3):393-400.

108. Perry EK, Tomlinson BE, Blessed G, Bergmann K, Gibson PH, Perry RH. Correlation of cholinergic abnormalities with senile plaques and mental test scores in senile dementia. British Medical Journal. 1978;2(6150):1457-9.

109. Bierer LM, Haroutunian V Fau - Gabriel S, Gabriel S Fau - Knott PJ, Knott Pj Fau - Carlin LS, Carlin Ls Fau - Purohit DP, Purohit Dp Fau - Perl DP, et al. Neurochemical correlates of dementia severity in Alzheimer's disease: relative importance of the cholinergic deficits. J Neurochem. 1995;64(2):749-60.

110. DeKosky ST, Harbaugh Re Fau - Schmitt FA, Schmitt Fa Fau - Bakay RA, Bakay Ra Fau - Chui HC, Chui Hc Fau - Knopman DS, Knopman Ds Fau - Reeder TM, et al. Cortical biopsy in Alzheimer's disease: diagnostic accuracy and neurochemical, neuropathological, and cognitive correlations. Intraventricular Bethanecol Study Group. Ann Neurol. 1992;32(5):625-32.

111. Pappas BA, Bayley PJ, Bui BK, Hansen LA, Thal LJ. Choline acetyltransferase activity and cognitive domain scores of Alzheimer's patients. Neurobiology of Aging. 2000;21(1):11-7.

112. Mesulam MM, Geula C. Overlap between acetylcholinesterase- rich and choline acetyltransferase-positive (cholinergic) axons in human cerebral cortex. Brain Research. 1992;577(1):112-20.

113. Davis KL, Mohs RC, Marin D, Purohit DP, Perl DP, Lantz M, et al. Cholinergic Markers in Elderly Patients With Early Signs of Alzheimer Disease. JAMA. 1999;281(15):1401-6.

114. Gilmor ML, Erickson JD, Varoqui H, Hersh LB, Bennett DA, Cochran EJ, et al. Preservation of nucleus basalis neurons containing choline acetyltransferase and the vesicular acetylcholine transporter in the elderly with mild cognitive impairment and early Alzheimer's disease. Journal of Comparative Neurology. 1999;411(4):693-704.

115. Herholz K, Weisenbach S, Kalbe E, Diederich N, Heiss W. Cerebral acetylcholine esterase activity in mild cognitive impairment. Neuroreport. 2005;16(13):1431-4.

116. Herholz K. Acetylcholine esterase activity in mild cognitive impairment and Alzheimer's disease. Eur J Nucl Med Mol Imaging. 2008;35 Suppl 1:S25-9.

117. Haense C, Kalbe E, Herholz K, Hohmann C, Neumaier B, Krais R, et al. Cholinergic system function and cognition in mild cognitive impairment. Neurobiology of Aging. 2012;33(5):867-77.

118. Rinne JO, Kaasinen V, Jarvenpaa T, Nagren K, Roivainen A, Yu M, et al. Brain acetylcholinesterase activity in mild cognitive impairment and early Alzheimer's disease. J Neurol Neurosurg Psychiatry. 2003;74(1):113-5.

119. Johnson NA, Rademaker A, Weintraub S, Gitelman D, Wienecke C, Mesulam M. Pilot trial of memantine in primary progressive aphasia. Alzheimer disease and associated disorders. 2010;24(3):308.

120. Kertesz A, Morlog D, Light M, Blair M, Davidson W, Jesso S, et al. Galantamine in frontotemporal dementia and primary progressive aphasia. Dementia And Geriatric Cognitive Disorders. 2008;25(2):178-85.

121. Dickerson B. Quantitating Severity and Progression in Primary Progressive Aphasia. J Mol Neurosci. 2011;45(3):618-28.

Supplementary material

Table S-I. Characteristics per subgroup.

	Mild cognitive impairment	Healthy controls	Primary progressive aphasia
Age (mean±SD)	66.4 ±6.9 years	65.6 ±5.6 years	68 ±7.4 years
Gender			
Male	6	6	8
Female	2	3	4
Mean CDR score	0.5	0	1
Scans			
Baseline	n=8	n=9	n=12
Second	n=4	n=5	n=9
Time interval (mean±SD)	366±63 days	727± 72 days	376±59 days

Abbreviations: CDR= clinical dementia rate and SD= standard deviation.

Table S-II. Regions of the AAL atlas.

Brain region	Associated VOIs per region	Hemisphere	Size (cc)
Frontal cortex	Precentral gyrus	L & R	11.28
	Superior frontal gyrus	L & R	11.328
	Superior frontal gyrus, orbital	L & R	4.4
	Middle frontal gyrus	L & R	18.144
	Middle frontal gyrus, orbital	L & R	4.056
	Inferior frontal gyrus, opercular	L & R	4.392
	Inferior frontal gyrus, triangular	L & R	8.216
	Inferior frontal gyrus, orbital	L & R	7.568
	Rolandic operculum	L & R	5.048
	Supplementary motor area	L & R	7.712
	Olfactory cortex	L & R	0.448
	Superior frontal gyrus	L & R	11.328
	Superior frontal gyrus, orbital	L & R	4.4
	Gyrus rectus	L & R	3.768
	Paracentral lobule	L & R	3.136
Temporal cortex	Heschl gyrus	L & R	0.88
	Superior temporal gyrus	L & R	10.904
	Temporal pole superior gyrus	L & R	3.4
	Middle temporal gyrus	L & R	21.944
	Temporal pole middle gyrus	L & R	3.352
	Inferior temporal gyrus	L & R	16.24
Parietal cortex	Postcentral gyrus	L & R	12.368
	Superior parietal gyrus	L & R	6.36

	Inferior parietal gyrus	L & R	8.056
	Supramarginal gyrus	L & R	6.648
	Angular gyrus	L & R	6.688
	Precuneus	L & R	13.424
Occipital cortex	Calcarine fissure	L & R	7.632
	Cuneus	L & R	6.696
	Lingual gyrus	L & R	8.96
	Superior occipital lobe	L & R	5.96
	Middle occipital lobe	L & R	12.848
	Inferior occipital lobe	L & R	4.872
	Fusiform	L & R	9.44
Hippocampus+	Hippocampus	L & R	1
	Parahippocampal gyri	L & R	4.312
	Amygdala	L & R	0.208
Cingulum	Cingulate gyrus, anterior part	L & R	6.616
	Cingulate gyrus, mid part	L & R	10.128
	Cingulate gyurs, posterior part	L & R	1.432
Insula	Insula	L & R	6.616
Basal ganglia	Caudate nucleus	L & R	3.336
	Putamen	L & R	5.6
	Pallidum	L & R	0.832
Thalamus	Thalamus	L & R	3.896
Cerebellum	Cerebellum crus 1	L & R	13.608
	Cerebellum crus 2	L & R	10.664
	Cerebellum 3	L & R	0.704
	Cerebellum 4_5	L & R	5.704
	Cerebellum 6	L & R	11.328
	Cerebellum 7b	L & R	2.936
	Cerebellum 8	L & R	10.992
	Cerebellum 9	L & R	4.472
	Cerebellum 10	L & R	0.272
	Vermis 1_2	/	0.544
	Vermis 3	/	1.864
	Vermis 4_5	/	2.44
	Vermis 6	/	1.656
	Vermis 7	/	1.528
	Vermis 8	/	1.384
	Vermis 9	/	0.672
	Vermis 10	/	0.512

Table S-III. Mean regional rate constants at baseline, per subgroup and using the 2T3k+V_b^{cor} model.

Regions	K_1 (mL · min^{-1}· g^{-1})			k_2 (min^{-1})			k_3 (min^{-1})		
	Mean			Mean			Mean		
	PPA	**HC**	**MCI**	**PPA**	**HC**	**MCI**	**PPA**	**HC**	**MCI**
Frontal cortex	0.268	0.348	0.354	0.115	0.130	0.136	0.021	0.022	0.021
Temporal cortex	0.250	0.357	0.358	0.102	0.123	0.127	0.020	0.021	0.019
Parietal cortex	0.267	0.355	0.358	0.114	0.131	0.135	0.019	0.020	0.018
Occipital cortex	0.288	0.365	0.368	0.123	0.138	0.142	0.020	0.021	0.019
Hippocampus+	0.207	0.289	0.278	0.081	0.095	0.095	0.027	0.027	0.025
Cingulum	0.309	0.403	0.400	0.121	0.137	0.138	0.022	0.023	0.020
Insula	0.267	0.376	0.375	0.105	0.122	0.126	0.022	0.023	0.021
Basal ganglia	0.282	0.343	0.344	0.026	0.029	0.033	0.037	0.042	0.040
Thalamus	0.341	0.457	0.341	0.128	0.151	0.148	0.048	0.047	0.046
Cerebellum	0.277	0.341	0.333	0.072	0.079	0.083	0.067	0.067	0.062

Data are represented as mean values. The analysis was performed on a VOI-based level using the 2T3k+V_b^{cor} model in healthy controls. + Hippocampus and amygdala. Abbreviations: 2T3k+V_b^{cor} model= two-tissue three-rate constant model including a plasma fraction with a plasma input corrected for metabolites; PPA= primary progressive aphasia, HC= healthy controls; MCI= mild cognitive impairment and VOI= volume of interest.

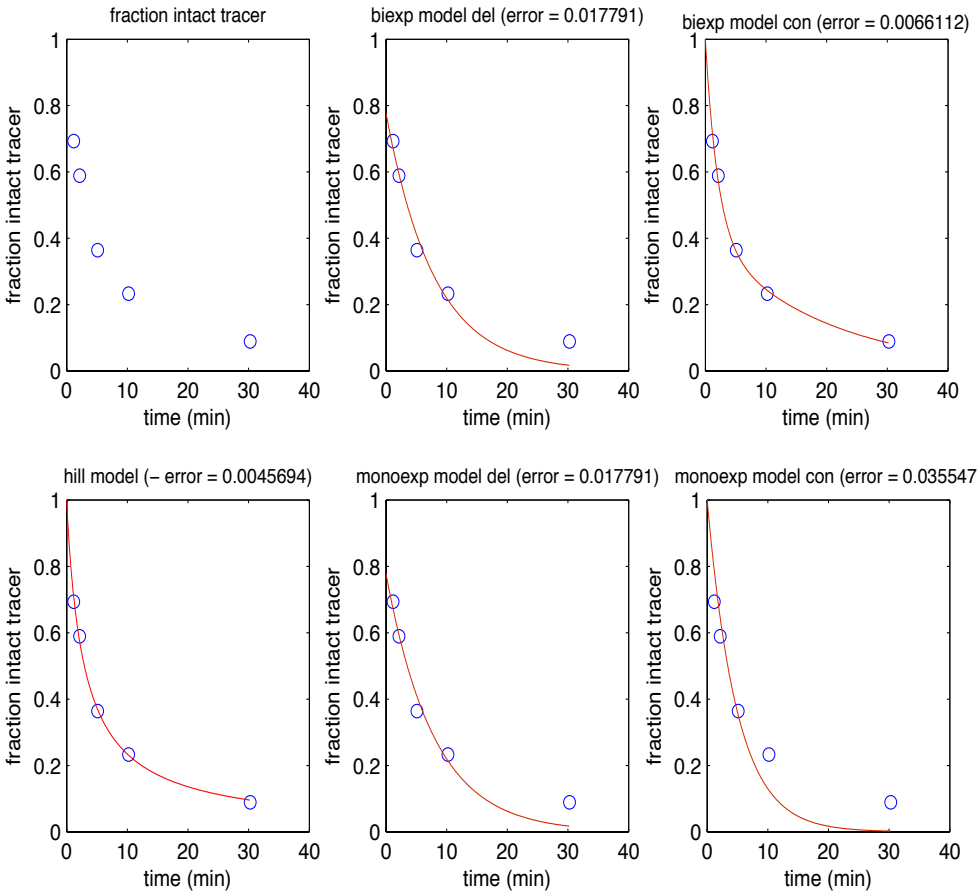

Figure S-I. Fits of the authentic PMP tracer fraction using five distinct functions. The analysis was performed in a healthy control. The error indicates the inaccuracy between the measured and fitted data. Abbreviations: biexp = bi-exponential; monoexp= mono-exponential; del= delay and con= constrained.